IOP Publishing Phys. Med. Biol. 65 (2020) 02TR01 (28pp) https://doi.org/10.1088/1361-6560/ab5507

Physics in Medicine & Biology

IPEM Institute of Physics and Engineering in Medicine

RECEIVED
28 May 2019

REVISED
5 September 2019

ACCEPTED FOR PUBLICATION
6 November 2019

PUBLISHED
16 January 2020

TOPICAL REVIEW

Technical advances in x-ray microbeam radiation therapy

Stefan Bartzsch[1,2], Stéphanie Corde[3,7,8], Jeffrey C Crosbie[4], Liam Day[4], Mattia Donzelli[5,6], Michael Krisch[5], Michael Lerch[7,8], Paolo Pellicioli[5,9,10], Lloyd M L Smyth[11] and Moeava Tehei[7,8]

[1] Department of Radiation Oncology, School of Medicine, Technical University of Munich, Klinikum rechts der Isar, Munich, Germany
[2] Helmholtz Centre Munich, Institute for Radiation Medicine, Munich, Germany
[3] Radiation Oncology Department, Prince of Wales Hospital, Randwick NSW, Australia
[4] School of Science, RMIT university, Melbourne, Australia
[5] The European Synchrotron Radiation Facility, Grenoble, France
[6] The Institute of Cancer Research, London, United Kingdom
[7] Centre for Medical Radiation Physics, University of Wollongong, Wollongong NSW, Australia
[8] Illawarra Health and Medical Research Institute, University of Wollongong, Wollongong, Australia
[9] Inserm UA7 STROBE, Grenoble Alpes University, Grenoble, France
[10] Swansea University Medical School, Singleton Park, Swansea, United Kingdom
[11] Department of Obstetrics & Gynaecology, University of Melbourne, Melbourne, Australia

E-mail: stefan.bartzsch@tum.de

Keywords: microbeam radiation therapy, dosimetry, synchrotron radiation, dose calculation, high dose rate

Abstract

In the last 25 years microbeam radiation therapy (MRT) has emerged as a promising alternative to conventional radiation therapy at large, third generation synchrotrons. In MRT, a multi-slit collimator modulates a kilovoltage x-ray beam on a micrometer scale, creating peak dose areas with unconventionally high doses of several hundred Grays separated by low dose valley regions, where the dose remains well below the tissue tolerance level. Pre-clinical evidence demonstrates that such beam geometries lead to substantially reduced damage to normal tissue at equal tumour control rates and hence drastically increase the therapeutic window. Although the mechanisms behind MRT are still to be elucidated, previous studies indicate that immune response, tumour microenvironment, and the microvasculature may play a crucial role. Beyond tumour therapy, MRT has also been suggested as a microsurgical tool in neurological disorders and as a primer for drug delivery.

The physical properties of MRT demand innovative medical physics and engineering solutions for safe treatment delivery. This article reviews technical developments in MRT and discusses existing solutions for dosimetric validation, reliable treatment planning and safety. Instrumentation at synchrotron facilities, including beam production, collimators and patient positioning systems, is also discussed. Specific solutions reviewed in this article include: dosimetry techniques that can cope with high spatial resolution, low photon energies and extremely high dose rates of up to 15 000 Gy s^{-1}, dose calculation algorithms—apart from pure Monte Carlo Simulations—to overcome the challenge of small voxel sizes and a wide dynamic dose-range, and the use of dose-enhancing nanoparticles to combat the limited penetrability of a kilovoltage energy spectrum. Finally, concepts for alternative compact microbeam sources are presented, such as inverse Compton scattering set-ups and carbon nanotube x-ray tubes, that may facilitate the transfer of MRT into a hospital-based clinical environment.

Intensive research in recent years has resulted in practical solutions to most of the technical challenges in MRT. Treatment planning, dosimetry and patient safety systems at synchrotrons have matured to a point that first veterinary and clinical studies in MRT are within reach. Should these studies confirm the promising results of pre-clinical studies, the authors are confident that MRT will become an effective new radiotherapy option for certain patients.

1. Introduction

Despite the technical and biological advances of modern radiotherapy, there are many types of cancer that have not seen significant improvements in prognosis. For example, paediatric diffuse intrinsic pontine glioma, an aggressive brainstem tumour, has a survival rate of less than 10% at two years following diagnosis (Hargrave *et al* 2006). Locally advanced pancreatic cancer and glioblastoma multiforme both have survival rates of less than 10% at five years (Stupp *et al* 2009, Siegel *et al* 2015). Chondrosarcoma, a notoriously aggressive cancer of cartilaginous cells, is usually resistant to both chemotherapy and conventional radiotherapy, making surgical resection—often amputation—the main effective treatment option (Bovée *et al* 2005, Cesari *et al* 2007, Riedel *et al* 2009). In these scenarios, the intrinsic characteristics of the disease, or the sensitivity of surrounding organs to radiation, hinders any opportunity for lasting disease control.

These dismal outcomes suggest that a paradigm shift could be required to improve prognosis and perhaps provide the possibility of cure. Spatially fractionated radiotherapy using microbeams is a radical departure from the physical properties and radiobiological principles of conventional radiotherapy. The purpose of this review is to explore the physics and technical developments fundamental to the field of microbeam radiotherapy (MRT).

1.1. Paradigms in modern radiation oncology

The broad aim of conventional radiotherapy is to safely deliver the highest possible homogenous dose to the target volume. This objective is primarily achieved through the temporal fractionation of dose and geometric dose-conformity to the target. Linear accelerators are the workhorse of modern radiotherapy clinics globally, facilitating the treatment of a diverse range of tumours in virtually any location in the body. Most linear accelerators generate mega-electron-volt (MeV) x-rays and electrons, operate at a dose rate in the order of 0.1 Gy s^{-1} and produce homogenous fields of radiation that can be collimated or modulated to optimise the geometry of dose-distributions in tissue.

Early in the 20th century, the first radiotherapy treatments were delivered as a large single fraction and associated with significant morbidity and physical disfigurement. These toxic effects were the backdrop for one of the most fundamental developments in radiation oncology; temporal fractionation. In the early 1920s, Claudius Regaud and his French compatriot Henri Coutard demonstrated that healthy tissue could better tolerate a course of radiotherapy when delivered as a series of several smaller doses over consecutive days, without compromising tumour control (Holsti 1995). Splitting a large radiation dose into multiple smaller fractions capitalises on four of the 'Five Rs of Radiotherapy' Hall and Giaccia (2012). In healthy tissue, there is opportunity for the repair of non-lethal DNA damage and repopulation of the normal cell niche. Simultaneously, the processes of reoxygenation and cell-cycle redistribution increase tumour radio-sensitivity. Temporal fractionation gained acceptance in the wider radiation therapy community by the 1930s and remains a cornerstone of modern radiation oncology.

The therapeutic effect of radiotherapy is also fundamentally maximised by increasing the geometric conformity of dose to the tumour target. Given that healthy tissue surrounding the tumour limits the maximum dose deliverable, the high-dose region is sculpted as closely as possible to the target volume. The target typically includes the gross tumour volume plus an additional margin in normal tissue to account for sub-clinical spread and uncertainties in target position. The majority of technical advancements in modern radiation oncology—intensity modulation (Fraass 1995, Boyer and Cedric 1999), image-guidance (van Herk 2007, Raaymakers *et al* 2017), motion-management (Lin *et al* 2013, Zagar *et al* 2017), particle therapy (Schulz-Ertner *et al* 2006)—have revolved around improving the conformity of dose to the target, reducing collateral damage to healthy tissue and facilitating dose-escalation.

1.2. Spatially fractionated radiotherapy

The concept of spatial fractionation is built on the dose-volume effect; that the tolerance of normal tissue to radiation increases as the irradiated volume of that specific tissue is reduced (Hopewell *et al* 1987, Emami *et al* 1991, Marks *et al* 2010). Alban Köhler first conceived the idea of applying spatial fractionation to radiotherapy in 1909. Köhler showed that skin toxicity could be reduced using 'grid therapy', where a 3 mm^2 grid of woven iron wire was pressed closely to the skin of patients during kilovoltage irradiation (Laissue *et al* 2012). Today, macroscopic grid therapy using megavoltage x-rays from a linear accelerator is used to de-bulk large and advanced tumours prior to conventional radiation therapy (RT) (Zhang *et al* 2008), however this technique is not widely used.

Several forms of spatially fractionated radiotherapy, including MRT, are currently in pre-clinical development. While MRT is the focus of this review, there are other noteworthy modalities including minibeam radiotherapy, which utilises arrays of sub-millimetre (0.4–0.7 mm) planar beams of x-rays (Gil *et al* 2011, Prezado *et al* 2012b, 2015) or protons (Peucelle *et al* 2015, Prezado *et al* 2017b), and microchannel irradiation using arrays of x-ray or proton microbeams (Schültke *et al* 2013, Girst *et al* 2015).

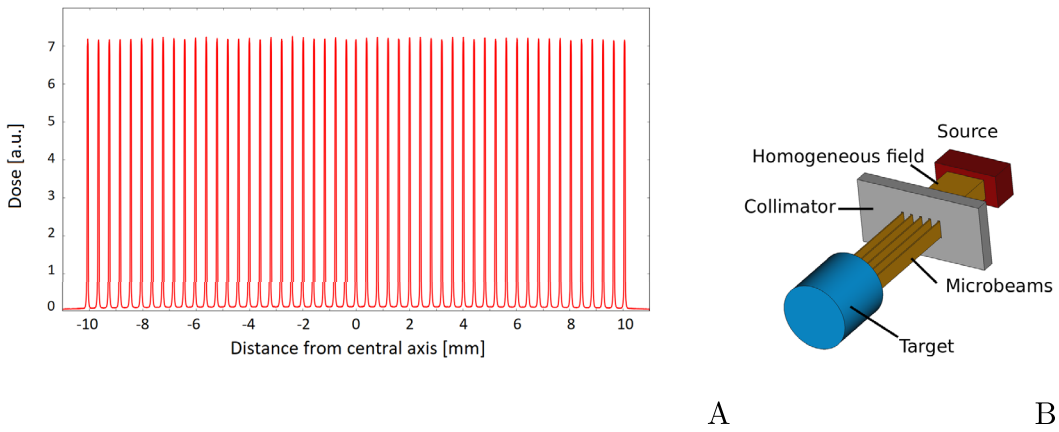

Figure 1. (A): A typical beam profile of microbeams, simulated for a 20 mm × 4 mm field in 10 mm depth in water at the imaging and medical beamline of the Australian Synchrotron. The principle of microbeam generation is shown in (B). A collimator shapes microbeams from a homogeneous x-ray beam.

1.3. Microbeam radiotherapy

At present, MRT is the most extensively investigated modality that employs spatial dose-fractionation. Microbeams were first used in medicine in the 1960s to understand the effects of cosmic radiation. At that time, Zeman *et al* (1961) reported that the tolerance of mouse brain tissue to a single beam of deuterons could be increased from 140 Gy to 4000 Gy when reducing the diameter of the beam from 1 mm to 25 μm. While the work of Zeman and colleagues exemplified the dose-volume effect, it was not until the late 1980s that true spatial dose-fractionation using microbeams was demonstrated.

MRT was first explored by Daniel Slatkin and colleagues at the Brookhaven National Laboratory in the late 1980s and early 1990s (Slatkin *et al* 1992, 1995). MRT has been in pre-clinical development at a small number of synchrotrons across the world ever since, including the European Synchrotron Radiation Facility (ESRF) (Grenoble, France), SPring-8 (Hyogo Prefecture, Japan), the Australian Synchrotron (Melbourne, Australia) and the Canadian Light Source (Saskatoon, Canada).

In MRT, spatial dose-fractionation is achieved on a microscopic scale. Fields are characterised by an array of 25–100 μm wide, quasi-parallel, micro-planar beams that have a centre-to-centre spacing of 100–400 μm (Bräuer-Krisch *et al* 2010). This kind of array creates an inhomogeneous, periodically alternating dose profile of 'peaks' and 'valleys' (figure 1). In-beam doses (peaks) can be up to 100 times higher than the dose between the beams (valleys) due to scatter (Blattmann *et al* 2005). In pre-clinical *in vivo* studies, peak to valley dose ratios (PVDRs) are more commonly in the range of 20–50 (Serduc *et al* 2009, Laissue *et al* 2013, Mukumoto *et al* 2017, Schültke *et al* 2018, Smyth *et al* 2018). The physical characteristics of MRT are discussed more thoroughly in sections 2 and 4.

Peak doses used in pre-clinical MRT experiments usually fall in the range of 100–1000 Gy (Schültke *et al* 2008, Serduc *et al* 2008, Laissue *et al* 2013, Ibahim *et al* 2014). These extremely high peak doses are tolerated by a range of healthy tissues with minimal structural or physiological deficits (Laissue *et al* 2007, 2013, Serduc *et al* 2008, Van Der Sanden *et al* 2010, Smyth *et al* 2018). In addition to the remarkable tolerance of normal tissue to peak doses, pre-clinical studies show that MRT can slow tumour growth and even facilitate tumour control despite not irradiating the entire tumour with a uniform field (Laissue *et al* 1998, Miura *et al* 2006, Bouchet *et al* 2016).

While compact MRT delivery systems have also been developed (Hadsell *et al* 2014, Bartzsch *et al* 2016) and are reviewed in section 6, the properties of synchrotron radiation are optimal for delivering the peak-valley dose-distribution intrinsic to MRT (Slatkin *et al* 1992). Firstly, the keV x-ray energy minimises the range of secondary electrons in the valley region, preserving a high PVDR. Secondly, the ultra high dose rate in the range of kGy/s mitigates the effects of physiological tissue motion, including the cardio-synchronous pulsation of blood vessels and respiration. Lastly, minimal beam divergence is required to maintain the array geometry on a microscopic scale. The high dose-rates and peak doses, in combination with microscopic spatial resolution, makes physical methods of dosimetry very demanding. Techniques to facilitate synchrotron-based MRT dosimetry are discussed in section 3.

There are a number of mechanisms that have been proposed for the therapeutic efficacy of MRT. Firstly, normal tissue retains its cellular architecture and the ability to launch a coordinated repair response following MRT while certain tumour tissues (e.g. breast tumour) demonstrate marked cellular migration and reduced proliferative capacity (Crosbie *et al* 2010). Secondly, MRT exerts differential transcriptomic effects on tumour and normal tissue, with differences in key pathways relating to immunity and inflammation (Bouchet *et al* 2013b, 2015).

The regulation of inflammation and immune response is also different when comparing tissue irradiated using MRT versus conventional RT (Sprung *et al* 2012, Yang *et al* 2014, Ibahim *et al* 2015), which further highlights the potential importance of these pathways to the therapeutic effect of MRT. Thirdly, tumour micro-vasculature has a greater radio-sensitivity to MRT compared to normal brain micro-vasculature (Bouchet *et al* 2010, 2013a), which has implications for vascular permeability and the delivery of micro-nutrients, cellular mediators of damage repair and immune cell recruitment. Finally, the ultra-high dose-rate of MRT—several hundred (Livingstone *et al* 2017) to several thousand (Renier *et al* 2008) Gray per second—may contribute to improved normal tissue sparing via what is now known as the FLASH effect (Favaudon *et al* 2014).

The degree to which the FLASH effect might contribute to the normal tissue sparing characteristics of MRT has not yet been elucidated. However, as a stand-alone technique, broad-beam FLASH radiotherapy at dose-rates greater than 40 Gy s^{-1} reduces lung fibrosis (Favaudon *et al* 2014) and mitigates brain injury (Montay-Gruel *et al* 2017, 2018) in rodent models compared to irradiation at conventional dose-rates (0.1 Gy s^{-1}). These tissue-sparing phenomena have since been reproduced in large animal models, with pet cats bearing spontaneous facial cancers also experiencing favourable tumour control outcomes following treatment with FLASH radiotherapy (Vozenin *et al* 2019).

1.4. Potential clinical applications of MRT in medicine

MRT is currently in a pre-clinical phase and to date, no human patients have been treated with MRT. The current challenge is to develop safe protocols that maximally exploit the unique radiobiological properties of MRT. A diverse range of potential clinical applications of MRT have been identified and explored through *in vivo* studies.

The biological rationale for MRT as a stand-alone, combination, or neoadjuvant treatment has been established in pre-clinical studies. Significant technical developments in the realm of medical physics are required to facilitate future pre-clinical and veterinary studies, and ultimately, the first human trials of MRT. These developments are the focus of this review.

1.4.1. MRT as a boost for conventional radiotherapy.

Schültke *et al* (2017) propose that MRT could be used as an integrated boost within a conventional radiotherapy regimen. Here, the valley dose would match the daily prescribed conventional radiotherapy dose while the peaks would act as a simultaneous boost to enhance tumour control (Schültke *et al* 2017). Bouchet *et al* (2016) provide a rationale for this approach by demonstrating better overall survival, in a rodent glioma model, following MRT compared to broad-beam irradiation when the MRT valley dose was matched to the broad-beam dose.

1.4.2. MRT as a primer for drug delivery

The previous potential applications of MRT largely draw on the normal tissue sparing properties of spatial fractionation, allowing for dose-escalation to the tumour. However, the differential effect of MRT on tumour and normal microvasculature (Bouchet *et al* 2010) makes MRT a potentially potent primer for drug delivery by inducing a window of enhanced vascular permeability in the tumour (Bouchet *et al* 2017). Similarly, the immunomodulatory properties of MRT (Bouchet *et al* 2013b, Yang *et al* 2014, Brönnimann *et al* 2016) could be exploited in combination with immunotherapy. Pre-clinical studies have demonstrated the synergistic effect of MRT in combination with a range of drugs (Régnard *et al* 2008, Bouchet *et al* 2012) and immunotherapy (Smilowitz *et al* 2006). However, the optimal dose and timing of MRT in this setting, and the choice of ideal chemo- or immunotherapeutics to test in combination, remains to be determined.

1.4.3. MRT as a micro-surgical tool in neurological disorders

Alongside possible applications in radiation oncology, MRT has the potential to alleviate the symptoms of neurological conditions. In this context, MRT could be used to deliberately transect key neuronal pathways or ablate highly localised regions of the brain in order to modulate or suppress the networks responsible for abnormal movement (Serduc *et al* 2010b, Romanelli and Bravin 2011). Proof of principle data supporting these neurosurgical applications of MRT exists in pre-clinical models of spinal cord injury (Dilmanian *et al* 2012) and epilepsy related to the somatosensory cortex (Pouyatos *et al* 2013). Epilepsy induced by mesial temporal sclerosis may also benefit from this application of MRT (Fardone *et al* 2018).

2. Technical development and engineering

2.1. Properties of synchrotron radiation

The discovery of synchrotron radiation in 1946 (Elder *et al* 1947) and the subsequent development of synchrotron radiation research centers around the world have revolutionized x-ray science. Modern synchrotron sources at dedicated storage rings have a brilliance (number of photons/s/mm^2/$mrad^2$ within a bandwidth of 0.1%) in the order of 10^{21} as compared to 10^7 for conventional x-ray tubes (Kim 1986, Duke 2009, Winick and

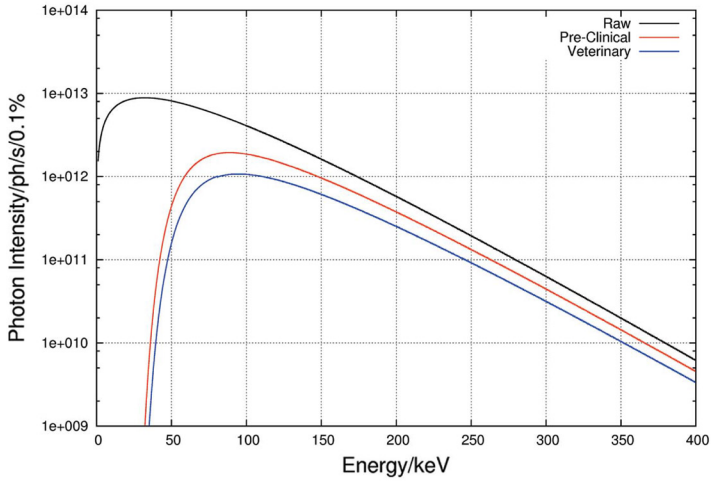

Figure 2. Typical unfiltered and filtered wiggler spectrum for MRT applications. Example of ID17 at the ESRF. Figure from Crosbie *et al* (2015) reproduced with permission of the International Union of Crystallography, https://doi.org/10.1107/S1600577515008115.

Doniach 2012). Currently, the most appropriate x-ray source for MRT is a so-called wiggler (as opposed to a bending magnet or an undulator), which provides a continuous high photon flux spectrum and a sufficiently large horizontal radiation fan for the desired size of the radiation field (see figure 2). The main considerations for the optimization of the MRT photon spectrum relate to (i) maximising the photon flux to allow for the required dose rate delivery; (ii) providing the necessary x-ray energy to reach deep-lying targets, and (iii) maximising the peak-to-valley-dose ratio (PVDR). In this context, photon energies below 50 keV are considered not useful; these are therefore filtered out by the insertion of a set of absorption filters (see below).

On the other hand, extensive MC calculations of an array of micro-beams revealed that a mean photon energy around 100–150 keV gives the best compromise between a well-defined peak dose profile with a sharp fall-off towards the valley dose region (Spiga *et al* 2007a, Donzelli *et al* 2018) (see section 4).

2.2. General beamline lay-out

The typical beamline lay-out for MRT has been described in detail in the past (Martínez-Rovira *et al* 2012b, Cornelius *et al* 2014, Wysokinski *et al* 2015, Stevenson *et al* 2017). Standard components comprise horizontal and vertical slits to reduce the heatload and to define the broad and MRT beam dimensions. A filter train eliminates the low-energy part of the spectrum. To monitor the beam stability, ionization chambers (IC) or a Compton chamber beam monitor are installed. Preclinical studies with small and large animals require slightly different conditions in terms of spectral filtering, intensity, and dose monitoring (Martínez-Rovira *et al* 2012b, Cornelius *et al* 2014, Crosbie *et al* 2015).

2.3. Fast shutters

The radiation dose delivered to the target, needs to be accurately controlled in order to prevent unnecessary damage to surrounding, normal tissues. Implementation of a dedicated photon shutter system, combined with a reliable, redundant interlock system, prevents any excessive dose delivery.

The system, implemented on the biomedical beamline ID17 at the ESRF, consists of a standard photon absorber, followed down-stream by a fast shutter device (Renier *et al* 2002). The measured error in the exposure time of the fast shutter amounts to ± 0.5 ms, which results in a 1% error for typical exposure times of 50 ms.

2.4. Multislit collimator

One of the key elements in MRT is the multislit collimator (MSC) since the mechanical regularity of such devices is the most important property required to produce an array of identical microbeams. Following first designs (Archer 1998, Bräuer-Krisch *et al* 2005a), the currently most utilized MSC is a single slit device composed of 8 mm thick blocks of tungsten carbide (WC), presenting 125, three mm high, and 50 μm wide equidistant slits to the incoming seamless x-ray beam, regularly repeated with a uniform pitch of 400 μm (Bräuer-Krisch *et al* 2009). The MSC chamber is mounted on a rotational stage, equipped with a motorized translation in the vertical direction and in the horizontal direction perpendicular to the x-ray beam, for rapid alignment. Schematic drawings of the MSC and its assembly are shown in figure 3.

An extensive characterization of the MSC led to 404 μm (SD 10 μm) for the regularity of the slit spacing, and 51.8 μm (SD 1.1 μm) for the slit width.

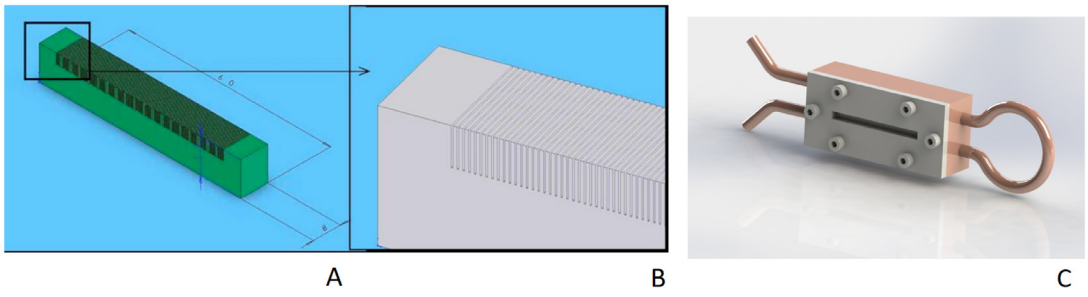

Figure 3. (A): Schematic drawing of a MSC with 100 μm slit width and a pitch of 400 μm and (B): zoom of the assembly; (C): MSC embedded inside the copper block with its pipes for water cooling.

2.5. Sample goniometer and patient positioning system

Sample and patient positioning systems for MRT are different from positioning systems used in conventional RT due to the use of a fixed horizontal beam rather than a rotating gantry. In addition, the limited beam height requires the vertical translation of a target through the beam during irradiation. At the ESRF a kappa-type goniometer manufactured by Huber (Germany) is installed (Bräuer-Krisch *et al* 2005a, Bräuer-Krisch *et al* 2013) on top of a vertical translational stage (see figure 4(A). Its loading capacity is 35 kg, and the z-stage allows for a total vertical movement of 150 mm at a maximum linear speed of 150 mm s^{-1}. The accuracy in velocity of the translational stage allows for a dose delivery with an accuracy of 5%. In view of the upcoming human clinical trials, a conceptual design study was performed for a patient positioning system (see figure 4(B)). At the BMIT beamline of the Canadian Light Source (CLS) in Saskatoon, Canada, a large animal positioning system (LAPS) is installed capable of holding samples up to 907 kg (Wysokinski *et al* 2015). The LAPS can move at vertical velocities of up to 200 mm s^{-1} at 1% accuracy and a spatial accuracy of 100 μm. On top of the LAPS a kappa-type goniometer with a loading capacity of up to 120 kg can be installed for 3-axis sample positioning (Wysokinski *et al* 2013) (see figure 4(C)).

More recently, the IMBL at the Australian Synchrotron have installed two robotic positioning devices; a so-called large animal positioning system (LAPS) and a Patient Positioning System (PPS) (see figure 4(D)). These robots are located in the long beamline known as Hutch 3B where phase contrast radiography, tomography, and some radiotherapy experiments take place. There are also plans to install another robotic patient positioning device on the near beamline (Hutch 2B) in the future. These robots are similar in scale to the positioning systems used in fixed-beam proton therapy facilities. Whilst these robotic devices are primarily used to image large animals and humans, they can also be used to translate patients vertically through a therapeutic beam. Commissioning work is taking place in 2019 to verify and validate the use of the LAPS and PPS for veterinary trials of synchrotron radiotherapy.

An irradiation sequence starts with the prepositioning of the target, and taking into consideration location marks obtained during prior imaging sessions. By means of the z-stage, the target is driven to the start position, and when the irradiation scan is triggered, the target accelerates vertically to reach the steady speed as chosen by the operator. The fast shutter opens and closes precisely at pre-determined positions depending on the volume to be treated. The target then decelerates and stops, and returns to its start position. The target may be re-oriented in another direction and a further irradiation sequence may start.

2.6. Image-guidance

Image-guidance is a well established technique in conventional RT to increase the spatial precision of a RT treatment. Various imaging techniques (fan and cone beam CT, x-ray projection imaging, MRI) can be used to verify the patient anatomy for planning and the patient set-up prior to and during the treatment.

The special circumstances at the currently available radiation sources for MRT have lead to the development of specialised techniques and protocols for image-guidance adapted to the fixed horizontal beam geometry at synchrotron facilities.

The first image-guided MRT experiment was reported in Serduc *et al* (2010a) by Serduc *et al* (2010a) at the ESRF beamline ID17. Their image-guidance protocol used the same radiation source for rat imaging and irradiation. To reduce the x-ray beam intensity and energy, the wiggler gap was opened and additional absorbers were placed in the beam for imaging. The rat imaging was carried out step by step acquiring 1 mm high frames while the animal was translated gradually upwards. A graphical user interface (GUI) displayed the full x-ray image and assisted in the positioning of the animal in the beam using bone structures of the skull as reference points for atlas-based alignment. The rotation was not corrected in this protocol which was used for radiosurgery of

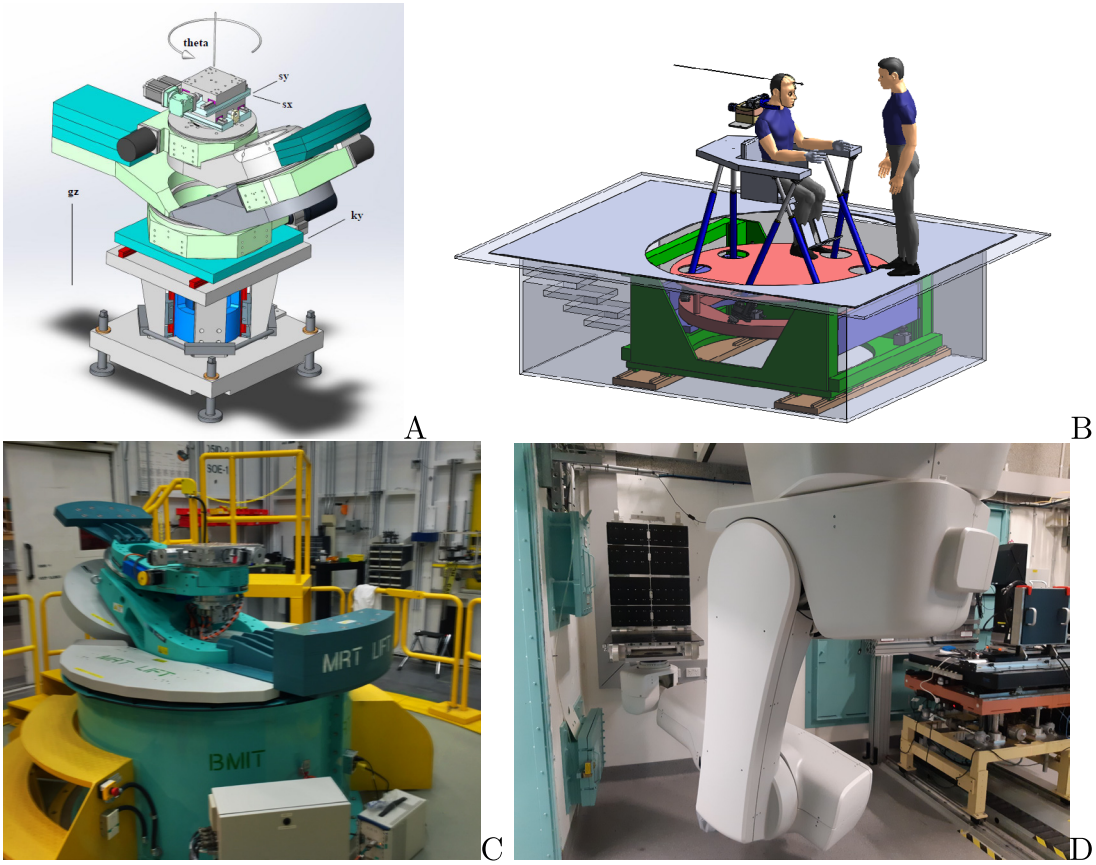

Figure 4. Current MRT kappa type goniometer in the MRT experimental hutch for preclinical research in MRT (A) and design of the future patient positioning and irradiation system for MRT clinical trials (B) at the ESRF. A stage for horse MRT trials at the Canadian Lightsource (C). A robotic patient positioning system (PPS) and a large animal positioning system (LAPS) has been installed at the Australian Synchrotron (D).

somatosensory cortex and thalamus of GAERS rats to investigate the effect of microbeams on epileptic seizures. The same protocol was successfully applied by others, e.g. Romanelli *et al* (2013).

Zhang *et al* (2014) used a combination of x-ray projection imaging and pre-irradiation MRI for tumour-bearing rats. They located the tumour on an MRI-image and performed an image-registration of sagittal MRI planes with projection images taken of the animal mounted on the irradiation stage of a carbon nano tube (CNT) based irradiator (Hadsell *et al* 2013). The applied re-positioning consisted of a translation of the animal in the image plane without any correction for the rotation.

The protocol developed by Nemoz *et al* (2016) at the ESRF was the first to acquire a full tomographic scan of the region of interest of a rat while the animal is immobilized on the treatment stage. Using a pink synchrotron radiation beam as described in Serduc *et al* (2010a), a CT of the animal head was acquired in 5 slices of 2 mm height each with a pixel size of 100 μm. Iodine as contrast agent was used to enhance tumour contrast on the CT images and the imaging spectrum was adjusted to match the iodine K-edge at 33 keV.

At the Australian Synchrotron (Pelliccia *et al* 2016b) developed a small animal image-guidance protocol which employs monochromatic synchrotron radiation for sample imaging. The use of a double-crystal Laue monochromator introduced a 20 mm shift between treatment and imaging beam which required vertical translation of the target in between the two procedures.

The sample imaging was done during a continuous vertical translation through the laminar x-ray beam, while a silicon detector acquired a series of images which were then tiled together to a full-field representation of the sample. To gather additional information on the sample, a CT slice of the plane selected on the projection image can be taken, similar to the procedure of Nemoz *et al* (2016). The image quality can be improved by relying on phase contrast images (Pelliccia *et al* 2016a). In addition the recent installation of an independent, external x-ray tube for full-field imaging at the Australian Synchrotron (Livingstone *et al* 2017), which is orientated perpendicularly to the synchrotron beam, may accelerate the procedure and overcome the impractical translation of the target between imaging and treatment.

The first alignment protocol for large animals was developed for ID17 at the ESRF by Donzelli etal (2016). The protocol was based on individual treatment planning where the target and the beam directions were defined on a CT image with the help of a commercial treatment planning platform. The alignment of the target used

fiducial markers as reference points, which were placed on the animal during CT-imaging. Before the treatment, x-ray projection images of the animal on the treatment stage were acquired from different angles. With the aid of manually identified fiducial markers in these projection images, an algorithm calculated the correct translation in 3 dimensions and rotation about 3 axes to be applied to have the beam orientation as defined in the treatment plan. This protocol was used successfully to irradiate small pigs at ID17 in February 2017.

2.7. Organ motion

Organ motion during irradiation can have a serious impact on microbeam dose distributions. The impact of dose blurring has been assessed with MC studies by Donzelli (2018) and Manchado de Sola *et al* (2018). Donzelli *et al* (2016) investigated the effect of cardiovascular brain motion during MRT treatment and came to the conclusion that dose rates of 12.3 kGy s^{-1} are necessary to ensure steep dose penumbras. Such high dose rates currently force any clinical applications to be carried out at large synchrotron facilities. Beyond blurring, organ motion is also hazard when aligning microbeam arrays applied from different directions. In preclinical studies so called interspersed geometries have been created to form almost homogeneous doses in the tumour target (Bräuer-Krisch *et al* 2005b). It is questionable whether such beam geometry can be reliably applied in clinical applications.

Organ motion introduces considerable risk of misalignment, particularly for interlaced microbeam patterns. Donzelli *et al* (2019) introduced a concept called spiralMRT, a geometry offering similar spatial fractionation properties as interlaced MRT, while being less vulnerable to target positioning uncertainties. The dose distributions achievable with spiralMRT in a simplified human head geometry were calculated with Monte Carlo simulations based on Geant4 and the dependence of the result on the microbeam pitch, total radiation field size, and photon energy were analysed. A comparison with interlaced MRT and conventional MeV tomotherapy was carried out.

SpiralMRT delivers homogeneous dose distributions to the target, while using spatially fractionated entrance beams. The valley dose of spiralMRT entrance beams is by up to 40% lower than the corresponding tomotherapy dose. SpiralMRT thus offers to be a promising approach to delivering homogeneous dose distributions with spatially fractionated entrance beams, possibly decreasing normal tissue side effects in hypofractionated radiation therapy.

3. Dosimetry

Experimental dosimetry is an essential ingredient, together with state-of-the-art dose calculations, for the development and validation of the TPS. The main challenges in MRT dosimetry are on one hand to determine the very high dose rates in the homogeneous field on an absolute scale, taking into account the necessary corrections to be applied for the typical spectrum from a synchrotron radiation x-ray source, and on the other hand the dose measurement of an array of x-ray micro-beams, modulated on a micrometer scale.

Regarding absolute dose determination in a homogeneous field, ion chambers (section 3.1) are the accepted primary standard, while Alanine-based dosimetry (section 3.2) has obtained increased attention over the past years. This reference dosimetry is performed prior to the spatial fractionation of the x-ray beam, and Monte Carlo methods are used to convert the reference dose to the dose within the micro-beam field.

For micro-scale dosimetry (MSD), i.e. the determination of the absorbed dose with micrometer spatial resolution, commercially available Gafchromic® films are widely utilised, though there are certain limitations as will be detailed in section 3.3. This research has triggered several other developments in experimental MSD. During the last decade several detectors were tested for potential applications in MRT: samarium doped glasses (section 3.4), MOSFET edge-on and silicon strip detectors (section 3.5), high-resolution thermoluminescent dosimeter (TLD, section 3.6), polymer gels (Maryanski *et al* 1993, De Deene *et al* 2002, Bayreder *et al* 2006), Optical Computed Tomography (CT) using a radiochromic plastic named PRESAGE (Doran *et al* 2010), Fluorescent Nuclear Track Detectors (FNTD) (section 3.7), and optical fiber dosimetry (section 3.8). Most recently, the emergence of commercial, and clinically traceable diamond detectors with micron-scale spatial resolution have appeared on the market and are emerging as potential candidates for MRT dosimetry (section 3.9). Table 1 provides an overview of tested detector systems.

All of the above dosimetry technologies have specific strengths and weaknesses for the very demanding MRT dosimetry requirements. The Gafchromic® films, silicon detectors, TLDs, FNTDs and diamond detectors seem currently the most adequate and practical dosimeters. All are described in some detail below. Important for the application of microbeams is the determination of output or scatter factors that relate the dose rate in the homogeneous radiation field with the dose rate in the microbeam peaks. These factors are either determined by dosimetry or with Monte Carlo simulations and are a prerequisite for the precise dosage of MRT.

Table 1. Comparison of different high resolution dosimeters tested in MRT.

Detector	Operating range	Resolution	Dose rate dependence	Energy dependence	Measurement type
Radiochromic films	0.1 Gy–400 Gy	5 μm	None	Nearly tissue equivalent	Off-line, 2D
Sm doped glasses	1 Gy–1000 Gy	<1 μm	None	Medium	Off-line, 2D
MOSFET detectors	0.01 Gy–100 Gy	<1 μm	None	Strong	On-line, 2D
Silicon strip	Up to 100kGy	10 μm	Unknown	Strong	On-line, 1D
TLDs	0.01 Gy–500 Gy	5 μm	Unknown	Strong	Off-line, 1D
Polymer gels	0.01 Gy–100 Gy	100 μm	Strong above 5Gy min^{-1}	Low	Off-line, 3D
PRESAGE	10 Gy–500 Gy	20 μm	Unknown	Unknown	Off-line, 3D
FNTD	0.005 Gy–50 Gy	0.6 μm	None	Strong	Off-line, 2D
Optical fibre	Measures dose rate >10 Gy s^{-1}	10 μm	None	Medium	On-line, 0D
Diamond detector	Measures dose rate	1 μm	Low	Low	On-line, 0D

3.1. Ion chambers

Ionization chambers are the dosimetry standard tool in RT protocols for absolute dosimetry (Ma *et al* 2001, Siegbahn *et al* 2005). The validation of a treatment planning system (TPS) is usually done with ionization chamber measurements in a liquid water or solid water phantom. A protocol for absolute dose measurements was put in place for MRT preclinical work (Fournier *et al* 2016). It is based on the International Atomic Energy Agency's TRS 398 absorbed dose-to-water protocol (Andreo *et al* 2000, Fournier *et al* 2016).

Reference dosimetry was performed with the PinPoint 31014 IC (sensitive volume of 0.015 cm^3) from PTW for a homogeneous field of 2 cm $\times$ 2 cm size and at a depth of 2 cm in a water tank.

The absolute dose in water under reference conditions is given by Andreo *et al* (2000):

$$D_{w,Q} = M_Q \times N_{D,w,Q_0} \times k_{Q,Q_0} \tag{1}$$

where M_Q is the raw reading from the IC corrected for the influence of the temperature and pressure, the polarization between the IC electrodes, the calibration of the electrometer and the ion recombination. Pressure and temperature have to be measured during dosimetry measurement. N_{D,w,Q_0} is the calibration factor for the beam quality Q_0 and k_{Q,Q_0} a factor that corrects for the difference between the beam quality Q_0 used for the calibration and the beam quality Q under which the measurements are performed.

3.2. Alanine dosimeters

Alanine, an amino acid (2-Aminopropanoic acid) is the sensitive material in alanine dosimeters. There are several types of alanine: L or S (+)-alanine, D or R (−)-alanine, beta-alanine etc, but for dosimetry α-Alanine is used ($C_3H_7NO_2$). A stable alkyl free radical $CH_3C \bullet HCOO^-$ is produced upon irradiation. The exposure of an amino acid to ionizing radiation causes the production of radicals of which the number of unpaired electrons is proportional to the absorbed dose over a wide dose range and can be measured by Electron Spin Resonance (ESR) spectroscopy (Poole 1996, Schweiger and Jeschke 2001). The measured signal is linear from approximately 2 Gy–200kGy. Though Alanine dosimetry is not recognised as a primary RT standard, it is widely accepted as secondary standard for absolute dose measurements (Anton 2005, Anton and Lelie 2009). A recent comparative study between PinPoint IC and alanine dosimetry for homogeneous fields revealed an overall agreement between the two methods for a delivered dose between 50 and 5000 Gy of better than 0.7%. The overall uncertainties of the alanine dose measurements were 3.08% and 2.80% at 2σ for alanine analysis with an EMX EPR spectrometer and an e-scan benchtop spectrometer, respectively (Soliman *et al* 2019).

3.3. Radiochromic film dosimetry

Radiochromic films are a common tool in modern radiation therapy dosimetry. Using films, it is possible to measure 2-dimensional dose distributions with sub-millimetric resolution, a fundamental part of treatment plan verification.

The core of the radiochromic dosimeter is a crystalline polyacetylene material responsible for a dose dependent change in optical density. Radiochromic films do not require any chemical treatment, have a weak energy dependence from keV to MeV energies, are dose rate independent and provide spatial resolution between 5 and 25 μm depending on the film type. Film dosimetry is a relative dosimetry method and films are usually calibrated with ionisation chambers under reference conditions.

In conventional RT, the dose variation of the radiation field occurs on a millimetric scale and the film analysis can be performed with a flatbed scanner, providing the required sub-millimetric resolution. The analysis of film irradiated with 50 μm wide microbeams requires a more powerful instrument. Protocols for radiochromic film read-out at the micrometer scale initially used microdensitometers (Crosbie *et al* 2008, Martínez-Rovira *et al*

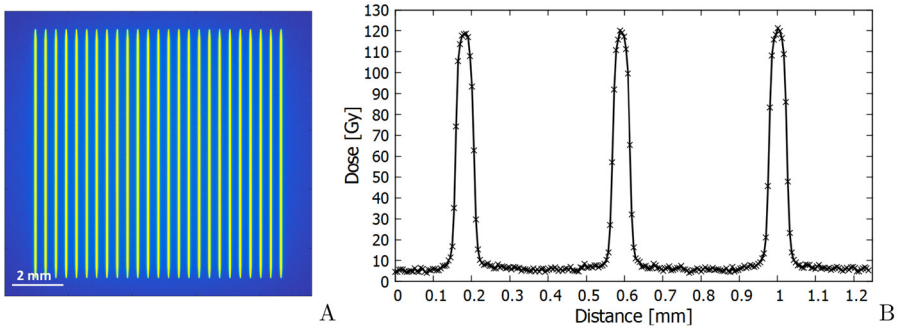

Figure 5. Digital image acquired with an optical inverted microscope of a HD-V2 Gafchromic® film irradiated with a 10 mm × 10 mm field of microbeams (A). Dose profile of 50 μm wide and 400 μm pitch microbeams (B).

2012b, Bräuer-Krisch *et al* 2015). The use of a microscope was suggested in 2009 by Nariyama *et al* (2009) and since then, developed protocols use an inverted optical microscope (Bartzsch *et al* 2015, Pellicioli *et al* 2019).

Microscopes equipped with motorized stages able to move with sub-micrometric precision combined with a charge-coupled device (CCD) camera, allow the acquisition of film areas up to 10 cm^2 in a few minutes with micrometric resolution and the evaluation of unusual field configurations such as pencil beams (Schültke *et al* 2013) or phantoms under motion conditions. Dedicated image processing protocols are being developed to correct the acquired digital images for noise and film inhomogeneities at the micrometric scale (Bartzsch *et al* 2015, Pellicioli *et al* 2019). An example of a digitalized film image is reported in figure 5. From the film analysis, dose profiles are obtained with a reproducibility of 1% and read-out uncertainties of less than 5%.

3.4. Samarium doped glasses

Another optical method with a resolution of better than 1 μm are glasses doped with certain rare earth atoms (Okada *et al* 2011). Especially the conversion of Sm^{3+} to Sm^{2+} has been studied for x-ray dosimetry, since the emission bands in the red part of the optical spectrum are well separated and changes in the fluorescence emission are easily accessible. The spatial variation of radiation dose on the micrometre scale can be read-out using confocal fluorescence microscopy. The detectors are reusable via reconversion of Sm^{2+} to Sm^{3+} by thermal annealing (Vahedi *et al* 2012) or exposure to UV-light (Okada *et al* 2014). Importantly, the dosimeters show a linear response in a wide dose range from cGy up to 150 Gy and are usable as non-linear dosimeters up to several thousand Gy (Vahedi *et al* 2012, Okada *et al* 2014).

3.5. Silicon detectors

Radiation dosimetry in conformal radiotherapy using silicon diodes is well documented in the literature and accepted in the clinical medical physics field. The physical parameters of the MRT beams, however, make it impossible to use such commercial silicon diodes for dosimetry. MOSFET detectors provide a high spatial resolution because of their very small radiation sensitive area defined by the thickness of the MOSFET gate oxide layer. Edge-on MOSFET dosimetry is a technique whereby a MOSFET radiation detector is positioned such that its smallest dimension is normal to the incident beam (Rosenfeld *et al* 2001).

At the ESRF profiles of a 30 μm wide microbeam were successfully acquired using the detector (Rosenfeld *et al* 2001). The MOSFET detector was also used for measuring the peak and valley doses (Bräuer-Krisch *et al* 2003). In 2009, the study carried out by Siegbahn *et al* (2009) reported PVDRs obtained by MC simulations up to 50% higher than the experimental PVDR measured with a MOSFET detector. These discrepancies were mainly attributed to the energy dependence of the detector assuming that there was a significant difference between the photon spectrum in the MRT peak compared to the valley. The MOSFET energy dependence was also highlighted in various articles (Kron *et al* 1998, De Felici *et al* 2005, Cheung *et al* 2009).

A silicon single-strip detector (SSD) and associated readout electronics have been developed to allow for very high spatial resolution measurements of the instantaneous dose rate at the detector's position in a phantom (Lerch *et al* 2009, 2011, Petasecca *et al* 2011) (see figure 6). The SSD response can then be integrated to deduce the total absorbed dose. The dynamic range of the readout system is over five orders of magnitude, which is ideal for MRT dosimetry.

The SSD design is also suitable for MRT dosimetry where the intrinsic beam height is usually 500 μm and microbeam width is typically 50 μm. The single strip active pad area has dimensions of 250 μm to 900 μm long and 10 μm wide. The SSD is fabricated using ion implantation production techniques. The active layer is a 100 Ω cm p-type epitaxial layer that is 50 μm thick and grown on top of the 370 μm thick silicon substrate of resistivity (0.001 Ωcm) (Lerch *et al* 2011, Petasecca *et al* 2011).

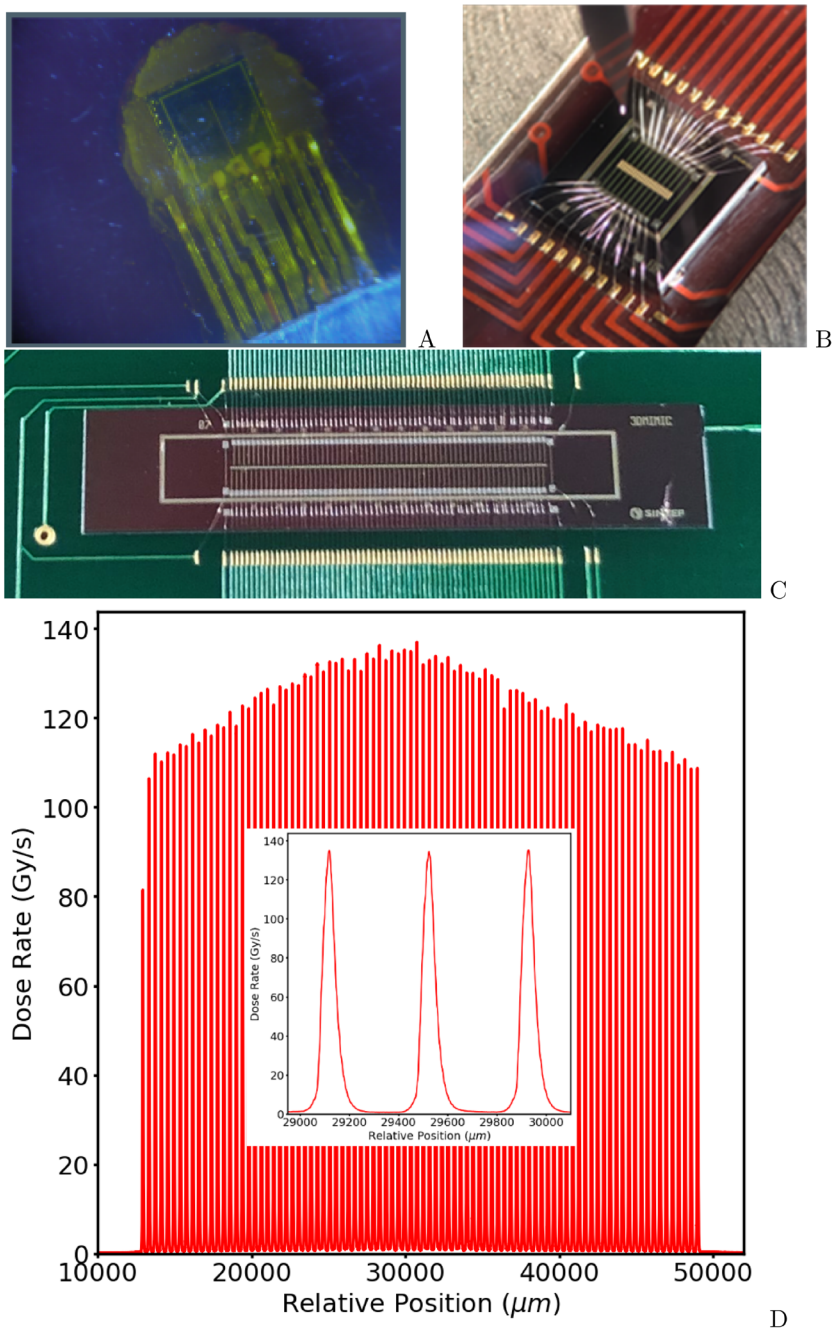

Figure 6. Generations of detectors developed for MRT dosimetry and QA. (A): Single silicon strip detector (SSD); (B): multi-strip silicon detector array (20 strips); (C): back-etched transmission silicon detector array (256 strip) for MRT QA; (D): typical 35 mm wide MRT treatment field map measured at the Australian Synchrotron by the SSD with a zoom of 3 microbeams overlayed.

In recent applications the SSD has been operated in passive mode where the spatial resolution is close to 20 μm in face-on mode. For the read out, a standard clinical electrometer can also be used. In this way, measurements can be more directly compared with other high resolution and clinically relevant dosimeters, under similar irradiation conditions (e.g. ionization chambers in broad beam conditions and other solid state detectors in microbeam conditions). Similar to the MOSFET devices, the best spatial resolution of the SSD of 5 μm is achievable when it is operated in passive mode, edge-on configuration and in good alignment with the microbeams (Fournier *et al* 2016, 2017). The combination of the SSD with the fast readout capability of the X-Tream dosimetry system and wide dynamic range allows for precise assessment of the MRT multislit collimator alignment to ensure the accurate reproducibility of the MRT irradiation field and associated dose delivery (see figure 6) (Davis *et al* 2018).

3.6. Thermoluminescence dosimetry

A two-dimensional (2D) thermoluminescence (TL) dosimetry system consisting of LiF : Mg, Cu, P (MCP-N)-based TL foils and a TLD reader equipped with a CCD camera and the large size (72 mm in diameter) planchete

heater was developed at the Institute of Nuclear Physics to perform high resolution dosimetry. TLDs have been used for MRT dosimetry; measured dose distributions were compared with Monte Carlo simulations. Measurments confirmed the findings obtained with Gafchromic films, particularly of a measured valley dose of 10%–40% higher than the Mont Carlo predicted dose (Ptaszkiewicza *et al* 2008).

3.7. Fluorescent nuclear track detectors

Fluorescent nuclear track detectors (FNTD) are a new type of luminescent detectors for different applications in radiation dosimetry. They were originally developed for neutron and heavy charge particle dosimetry (Akselrod *et al* 2006) and combine the advantages of solid state track detectors and optical measurements without the need for long chemical etching. The detectors are made of fluorescent aluminum oxide single crystals (sapphire) doped with carbon and magnesium ($Al_2O_3 : C, Mg$). The tracks of secondary electrons generated by the MRT beams in the single crystal aluminum oxide detector are imaged using a high resolution readout system based on confocal laser scanning fluorescence microscopy (Akselrod *et al* 2006).

FNTDs were optimized for imaging applications over 4 orders of magnitude of photon doses (Sykora and Akselrod 2010) ranging from 5 mGy to 50 Gy and extremely high spatial resolution of 0.6 μm. High spatial resolution and wide dynamic range of dose measurements make FNTD technology very attractive for MRT quality assurance application with a large PVDR (Bartz *et al* 2011). FNTD is a passive integrating type of detector that does not require wires, electronics or batteries during irradiation. This detector is immune to electromagnetic interference and can measure doses at very high dose rate; it was successfully tested at 108 Gy s^{-1}. FNTD detectors provide extremely good temperature and environmental stability, no light sensitivity, thermal fading or signal build-up. FNTD imaging plates are reusable after thermal annealing or optical bleaching. The most recent results obtained for MRT are summarized in Bartz *et al* (2011).

3.8. Fiber optical dosimeters

Fiber Optic Dosimeters (FODs) have a significant advantage over many dosimeters developed for MRT in that they are made of plastic scintillators. In an x-ray radiation field environment their water equivalence makes them excellent candidates for MRT and worthy of research and development. FODs typically find use in applications where high spatial resolution ($<$500 μm) is not essential since machining to very small thicknesses is very challenging and plastic scintillators have a low light yield (typically tens of thousands of photons per MeV of energy deposited). The synchrotron light source used in MRT can easily provide the necessary x-ray photon flux to facilitate a measurable response in FODs. However, Cherenkov radiation generation, radioluminescence, radiation hardness and dose rate dependence of FODs requires careful consideration if they are to be used regularly for MRT dosimetry.

Optical detectors have been applied to imaging microbeam x-rays in the past (Okada *et al* 2011, Belley *et al* 2015), however, they have not been used at highly brilliant synchrotron light sources. Archer *et al* (2017, 2018) have demonstrated a FOD probe development technique with improved spatial resolution using scintillators and have tested them in an MRT synchrotron x-ray beam, delivering very high dose rates. The scintillator thickness defines the one-dimensional spatial resolution of the FOD probe in the axial direction if it is operated in edge-on mode with respect to the direction and plane of the microbeams. The FOD length is 1 mm in the radial direction as determined by the optical fiber core diameter. The scintillation light generated in the plastic scintillator is transported along an optical fiber to a photomultiplier tube or silicon photomultiplier.

The most recently developed FOD has a one-dimensional spatial resolution of 10 μm. The detector is able to resolve the individual microbeams, and measure the peak-to-valley dose ratio that is consistent with other high spatial resolution detectors under the same irradiation conditions. The role of radioluminescence in the optical fibre used to transport the scintillation photons has been shown to create a significant contribution to the total light detected (Archer *et al* 2019).

3.9. Diamond detectors

Recently a solid state diamond detector, potentially suitable for use as a dosimeter in MRT, have become commercially available (Livingstone *et al* 2015, Marinelli *et al* 2016, Butler *et al* 2018). The PTW model 60019 'microDiamond^{TM}' (PTW-Freiburg GmbH, Freiburg, Germany) has a cylindrical active volume of 1.1 mm radius and 1 μm length. The microDiamond^{TM} is a synthetic single crystal diamond detector incorporating Schottky contacts, and is designed to be operated in passive mode with an electrometer (Almaviva *et al* 2010) .

Operation within the extreme radiation environment (very steep dose gradients, high dose rate, kilovoltage energy spectrum) typically used in MRT is well outside the conditions of use recommended by the manufacturer. However, excellent results have been demonstrated, particularly in the penumbra regions of the microbeams (Livingstone *et al* 2015). Very careful and precise alignment of the microdiamond is required to achieve such results. The device should be operated in edge-on mode to utilize the 1 μm thick active layer so as to fully exploit the best spatial resolution possible with this device.

4. Dose calculation and treatment planning

4.1. Physics of dose absorption in microbeam radiation therapy

Dose calculation and its validation by experimental data can be performed with high accuracy in conventional RT. Relative dose uncertainties in conventional RT are usually below 3% (Brahme 1984, Mijnheer *et al* 1987) and dose validation is part of international standards (ICRU Report 24 1976). In MRT, compliance with such high standards is challenging. The small sizes of the radiation fields, large differences between peak and valley doses and the low photon energies place extraordinary high demands on dose calculation and dosimetry. In this section we present various approaches and physical prerequisites for dose calculations in MRT.

MRT typically uses polychromatic x-ray beams with photon energies at around 100 keV. At these energies photons interact via photoelectric absorption, atomic Compton and Rayleigh scattering. Compton scattering is the most frequent photon interaction. Whereas MeV photons transfer the bulk part of their energy into kinetic energy of secondary electrons, the average energy transfer at low photon energy is rather low between 5 and 20%. Therefore multiple photon scattering substantially contributes to the scatter dose. Photoelectric absorption transfers almost all of the photon energy into kinetic energy of a secondary electron. The absorption coefficient of the photoelectric interaction strongly increases with decreasing photon energy and is particularly important for materials with atoms of higher atomic numbers.

Secondary electrons generated in photon interactions of primary, i.e. unscattered photons deposit their kinetic energy predominantly within the microbeam peak regions, due to short electron ranges. The dose in the valley is caused by electrons of primary photons scattering out of the peak region and electrons generated in interactions of scattered photons. If the spacing between microbeams is sufficiently high, i.e. higher than the typical electron range, the PVDR is closely proportional to the ratio of peak width to peak pitch (Hugtenburg *et al* 2010, Donzelli *et al* 2018)

The absorption coefficient of 100 keV photons is around 5 times higher than for 5 MeV photons. Hence depth dose curves are considerably steeper and the range of secondary electrons is much shorter than 1 mm. The build-up effect, which dominates the first centimeters of conventional MeV-photon RT depth dose curves affects 1 mm or less of the depth dose curves for 100 keV photon beams.

The choice of appropriate photon energies in MRT needs to balance between short electron ranges guaranteeing sharp beam penumbras and shallower depth dose curves allowing to irradiate deeper targets without an excess of surface dose. A shift of the photon spectrum to higher photon energies in a broad wiggler spectrum is usually achieved by adding additional filters. However, these filters also reduce the dose rate. The electron range does not gradually increase with photon energy but depends on the ratio between Compton and photoelectric effect. Since Compton electrons receive only part of the initial photon energy, their range is much shorter than that of photo electrons. Therefore beam penumbras decrease with increasing energies below and increase again above 100 keV photon energy. At 200 keV the Compton electron range reaches around 25 μm. A further increase of photo energy leads to a reduction of peak dose and PVDR of 50 μm wide beams. While photon energy is less relevant in small animal studies, future clinical applications may require slightly higher photon energies between 150 and 200 keV.

4.2. Monte Carlo dose calculation

In the past, the majority of MRT dose calculations were performed with Monte Carlo techniques. Early dose estimates involved homogeneous and simplified phantoms and in parts mono-energetic photon beams (Stepanek *et al* 2000). A wide range of different Monte Carlo codes has been used for dose calculations. First dose calculations were performed by Slatkin *et al* (1992) using an early EGS4 (INHOM) (Nelson *et al* 1985) version that includes transport of photons, electrons and delta-rays. However, only total ionization cross-sections were used in the electron transport ignoring the distribution of scattering angles and energies. Simulations in later EGS4 versions (Orion *et al* 2000, De Felici *et al* 2005, 2007) showed substantial deviations to these early calculations. Later Monte Carlo calculations used the PENELOPE framework (Martínez-Rovira *et al* 2012b, Prezado *et al* 2012a), a GEANT3 PSI-version (Stepanek *et al* 2000), GEANT4 (Spiga *et al* 2007a, Bartzsch *et al* 2014, Cornelius *et al* 2014), EGS5 (Hugtenburg *et al* 2010) and MCNPX (Hanson *et al* 2013). De Felici *et al* (2008) performed a comparison of different Monte Carlo codes and did not find differences in the dose distributions calculated with GEANT4, EGS4, EGS-NRC, PENELOPE and MCNPX. Due to flexibility and accuracy, Monte Carlo techniques have become the standard in MRT dose calculation.

Important parameters for precise Monte Carlo simulations are energy cut-off values for electron tracking and the choice of scattering cross section libraries. Particularly at low photon energies the shape of microbeam penumbras and the valley dose depend on the choice of physical models (Spiga *et al* 2007b). When working with synchrotron radiation, the chosen physics libraries should account for polarization effects. At the spatial scales of several micrometres condensed history simulations of the electron scattering are sufficient. Only at smaller volumes track structure simulations with tools such as GEANT4-DNA become necessary (Lazarakis *et al* 2018).

Small voxel sizes are a challenge for Monte Carlo simulations. The probability that a voxel is hit by a particle is proportional to its volume. In order to keep the statistical uncertainty constant the number of particle histories needs to be scaled inversely proportional to the voxel volume. In contrast to conventional RT, where voxel sizes of approximately 1 mm are sufficient, a multiport MRT treatment may need around 5 μm resolution in all spatial dimensions. This would require $8 \cdot 10^6$ times more particle histories and also memory than for Monte Carlo dose calculations in conventional radiotherapy. Therefore straight forward Monte Carlo simulations will not be feasible for MRT in the near future and strategies to overcome these challenges have to be provided. The majority of MRT dose calculations were performed for unilateral exposures and hence the voxel size can be reduced in only one spatial dimension (Siegbahn *et al* 2006, Martínez-Rovira *et al* 2012b). Other approaches use larger binning sizes and score peak and valley doses separately (Hugtenburg *et al* 2010, Debus *et al* 2017, Donzelli *et al* 2018), because anatomical information in a planning CT are provided on a coarse millimeter sized grid.

4.3. Simulation of radiation sources

An accurate description of synchrotron beam properties such as phase space and spectrum are a prerequisite for accurate dose calculation. Several early Monte Carlo studies assumed ideally parallel microbeams with equal beam intensity. Nettelbeck *et al* (2009) investigated the influence of beam divergence and the collimator on the simulated microbeams. They realized an increase in penumbral dose of up to 26% due to beam divergence, although differences in the peak and valley centre disappeared. Martínez-Rovira *et al* (2012b) did a complete simulation of the medical beam line of the ESRF from the wiggler to the multislit collimator and used the phase space for subsequent dose calculations.

Bartzsch *et al* (2014) characterized the phase space and showed that a simplified model of the phase space leads to microbeam dose estimates that do not differ measurably from a full phase space simulation. This model assumes parallel beams within the phantom or patient, leakage radiation in the valley regions behind the absorber material with a different spectrum and accounts for a change of flux due to partial shadowing and the lateral profile of the synchrotron beam intensity.

A special feature of synchrotron radiation is its almost total linear polarization which impacts on the atomic Compton and Rayleigh scattering of photons in matter. Since Rayleigh scattering leads only to small angle deviations of photon trajectories and is not creating secondary electrons, polarization will mainly influence dose distribution via Compton interaction. The differential scattering cross section of the Compton effect is given by the Klein–Nishina Formula

$$\frac{d\sigma}{d\Omega} = \frac{1}{4} r_0^2 \frac{E^2}{E_0^2} \left[\frac{E_0}{E} + \frac{E}{E_0} - 2 + 4\cos^2\Theta \right], \tag{2}$$

where E and E_0 are the photon energies of incoming and scattered photon, r_0 is the classical electron radius and Θ the angle between the polarization directions of incoming and scattered photon. Photons are preferentially scattered perpendicular to the polarization direction. One of the first investigating the effect of polarization were Orion *et al* (2000) using EGS4. Also De Felici *et al* (2005) used EGS4 to investigate how polarization effects the PVDR. They used 25 μm wide beams, 200 μm centre-to-centre spacing and 30 mm × 30 mm fields in a homogeneous water cylinder. Within the accuracy of the Monte Carlo simulations they did not see any polarization effects within the radiation field. Only in the photon scattering outside the microbeam field differences of up to 10% were observable. Hugtenburg *et al* (2010), on the other hand, came to the conclusion that polarisation effects are indeed essential for any future MRT treatment planning.

Studying the dose distribution around a pencil beam reveals how polarisation effects the dose distribution in microbeam fields (Spiga *et al* 2007b, Bartzsch *et al* 2014). Polarisation has a substantial impact on the direction of scattered Compton electrons and Compton photons and leads to a dose anisotropy. Photo electrons remain unaffected by photon polarisation and therefore dose absorption within the range of photo electrons is isotropic. As a consequence peak doses are almost unaffected by polarisation. Although the valley dose is dominated by Compton scattered photons, directional preferences level out within the microbeam field and polarisation corrections of the valley dose are between 1% and 3% in the field centre and field edge, respectively (Bartzsch *et al* 2014). Only in the scatter dose region outside the microbeam field substantial differences between polarized and unpolarized photons are observable (De Felici *et al* 2005, Hugtenburg *et al* 2010, Bartzsch *et al* 2014).

Despite considerable work and effort for precise dose calculations and dosimetry, substantial deviations between calculation and measurement have repeatedly been reported. Usually calculations are overestimating the PVDR and valley doses in measurements are 10 to 20% higher than predicted in simulations. Various effects may cause these deviations. Frequently discussed are influences of the multislit collimator. Although scattering from the collimator into the valley seems to be negligible (Nettelbeck *et al* 2009, Bartzsch *et al* 2014) simulations may induce unacceptable simplifications, such as perfectly plane surfaces. In fact a chemical analysis of the collimator surface of the biomedical beamline at the ESRF revealed substantial amounts of surface depositions, in particular copper. The fabrication process of the multislit collimator itself is challenging (Bräuer-Krisch *et al*

2009) and may infer variations in the peak width and peak distances which are not modelled in Monte Carlo simulations.

Furthermore Monte Carlo simulations neglect usually the wave nature of the particles they track, such as refraction, diffraction and total external reflection. Even hard x-rays have a refractive index which is slightly different to 1. At 100 keV this difference is in the order of $3 \cdot 10^{-7}$ (Kuznetsov 2014) leading to a critical angle for total external reflection of around 0.8 mrad. Due to the low divergence of the synchrotron beam, this angle is large enough to cause total external reflection at the collimator walls even for the outermost beams of a 30 mm × 30 mm field. Future investigations are required to reveal the cause of remaining discrepancies between simulation and measurement.

4.4. Alternative dose calculation methods

4.4.1. Semi-adjoint Monte Carlo simulations

As mentioned in section 4.2, the main problem when applying Monte Carlo tools to MRT are the required small voxel sizes. Monte Carlo problems with small detector volumes or when studying variable sources are often treated in their adjoint form Irving (1971) and Iván Lux (2000). Mathematically, Monte Carlo simulations can be seen as an integration of the Boltzmann transport equation (Iván Lux 2000). In the adjoint version of this integro-differential equation, detector and source term exchange their position. Hence, in the adjoint Monte Carlo simulation all 6 phase space dimensions of detector and source are swapped and interactions are tracked 'backwards in time'.

For MRT, the detector volume is small in the two dimensions perpendicular to the beam propagation. The MSC, as photon source has a large phase-space extension perpendicular to the propagation direction, while the source is small in all other phase space dimensions. Therefore the adjoint Monte Carlo problem will not lead to an advantage. However, it is possible to formulate a semi-adjoint version of the Monte Carlo problem exchanging only the two spatial dimensions perpendicular to the beam direction (see figure 7). As the momentum dimensions of detector and source remain unchanged in the phase space, particles can be tracked 'forward in time'. However, this partially adjoint version of the Boltzmann transport equation can only be derived if the phase space variables clearly separate, restricting this method to problems which are homogeneous perpendicular to the propagation direction and demand material homogeneity.

Theoretical derivations of this problem may be found in the respective literature dealing with Monte Carlo techniques and the Boltzmann transport equation. Here we only provide a brief heuristic explanation. Consider a photon emitted from the source element dS in the forward Monte Carlo problem in figure 7(A). The probability that a certain energy fraction dE of this photon is absorbed in the detector volume element dV_D is equal to the probability that the same energy fraction dE of a photon leaving the semi-adjoint source element dS' in figure 7(B) is absorbed in the semi-adjoint detector element dV'_D. More complicated source and detector geometries can be considered as compositions. If the number of particles emitted per source volume is equal for all source elements, the expectation of energy absorption in the forward detector and semi-adjoint detector will indeed be equal.

This method was employed by various authors (Hugtenburg *et al* 2010, Schültke *et al* 2013, Bartzsch *et al* 2014, 2015). It is particularly useful to determine so called relative output or scatter factors (ROF). With a single simulation it is possible to calculate ROFs for various field shapes. However, the restriction of this method to slab geometries limits its use in MRT treatment planning.

4.4.2. Kernel based dose calculation approaches and hybrid dose calculation

Despite a wide spread use of kernel based dose calculation algorithms in conventional RT for MeV photons, such algorithms are rarely used in the low energy x-ray domain below 1 MeV. In order to deal with tissue inhomogeneities, existing kernel based algorithms employ O'Connor's electron density scaling method (O'connor 1957, Mackie *et al* 1985, Bortfeld *et al* 1993), which is not applicable at low photon energies. Nevertheless, kernel based dose calculation methods for lower photon energies (Alaei *et al* 2000, 2010, Carlsson and Ahnesjö 2000) and also for MRT (Bartzsch and Oelfke 2013, Debus *et al* 2017) have been developed. Such kernel based dose calculation algorithms are capable of calculating microbeam dose distributions within five minutes and further acceleration seems technically feasible (Debus *et al* 2017). However, comparisons with Monte Carlo simulations show larger deviations, particularly in the valley regions.

Accurate and fast dose calculation can be achieved by combining kernel based and Monte Carlo based techniques in a hybrid approach. Problematic for kernel based dose calculation is the scattering of photons in inhomogeneous material. On the other hand, the tracking of secondary electrons on a micrometre scale is time consuming for Monte Carlo calculations. Photon scattering on a millimeter grid can be computed very efficiently, even within a few seconds as demonstrated in the past (Badal and Badano 2009, Jia *et al* 2010, 2012). Kernel algorithms can calculate the electron scattering with high accuracy assuming homogeneous material. Information on tissue inhomogeneities are given on a coarse millimeter sized grid.

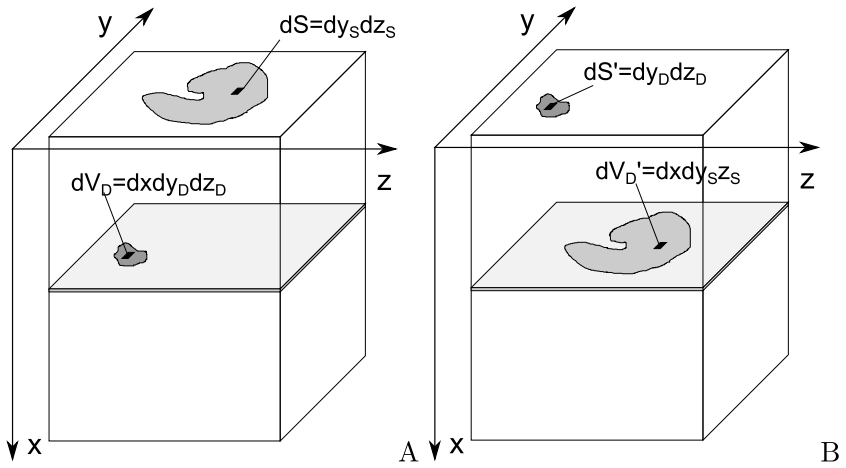

Figure 7. Forward (A) and semi-adjoint (B) Monte Carlo transport. An exchanging of source and detector geometry in the $y-z$-plane will lead to the same expected energy absorption in the detector, if the number of particles per source area is identical. Prerequisite is the homogeneity of the phantom in the $y-z$-plane.

In a hybrid dose calculation approach, Monte Carlo methods are used to calculate primary and scatter photon dose on a millimeter grid without considering electron scattering. In a subsequent electron convolution algorithm the microbeam pattern is calculated. Donzelli *et al* (2018) were able to show that such algorithms are around 600 times faster than pure Monte Carlo simulations and that there are no relevant differences in the calculated dose distributions when compared to pure Monte Carlo. Polarization effects and source phase space can be easily integrated into such hybrid methods.

4.5. Treatment planning

MRT treatment planning has to overcome several challenges compared to conventional RT. The dose needs to be calculated on very small spatial scales. As described above this requires specialized methods in dose calculation, but also storage and visualization of the calculated dose distribution deserves extra considerations. Quality assurance criteria such as the Γ index consider absolute dose changes or dose changes relative to the maximum dose (Low *et al* 1998). Since the Valley doses are only 5% of the peak dose, a valley dose accuracy of only 10% would require a very strict dose accuracy in the Γ-index of only 0.5%. Another challenge is the low photon energy and the related sensitivity to material composition. This requires special care when converting CT Hounsfield units into material composition for dose calculation.

Most preclinical studies in MRT used a few summary measures to characterize the dose distribution such as peak dose, valley dose or PVDR. Such measures can be calculated and visualized on a conventional millimeter sized grid. The definition of peak and valley dose requires some, often neglected attention, though. All dose measurements and calculations provide dose values on a finite grid and therefore some form of spatial averaging. However, because the doses vary on very small length scales, peak and valley doses should always be reported together with the applied averaging or voxel sizes for comparison. It would be desirable to establish standards on how peak and valley doses are presented.

The relevant radio-biological dose measure in MRT is a matter of ongoing research. Early studies in MRT usually used peak dose to compare biological results (Slatkin *et al* 1995, Laissue *et al* 2001, Serduc *et al* 2006, 2008), since peak dose is the easiest accessible quantity. More recent results show, however, that rather the valley dose is deciding on biological effects (Serduc *et al* 2009, Bouchet *et al* 2016), tumour control and tissue damage. A typical configuration of a microbeam exposure is 50 μm wide beams with a spacing of 400 μm. 'Perfect microbeams' with a sufficiently high peak dose and no valley dose, would kill 1/8th of the cells in the microbeam peaks and leave 7/8th of the cells in the valleys unaffected. A reduction of cell survival by 1/8th would correspond to only a few cGy homogeneous dose. Hence, the valley dose will mainly determine clonogenic cell survival if intercellular communication can be ignored.

Under the assumption that the clonogenic cell survival is determining tissue damage or tumour control and that only dose decides upon the fate of a cell, i.e. no bystander mechanisms, the equivalent uniform dose (EUD) (Niemierko 1997) would be the optimal parameter for MRT treatment planning as suggested by Meyer *et al* (2017). The advantage of this measure is its independence of beam geometries. For any microbeam dose pattern, even in cross firing regions the EUD can be calculated upon voxel based dose volume histograms as suggested by Donzelli *et al* (2018) (see figure 8).

Dose calculation algorithms have been coupled to TPS as in conventional RT. Such systems allow to define target volumes in CT-images of future patients, the adjustment of beam parameters such as field size, filtering,

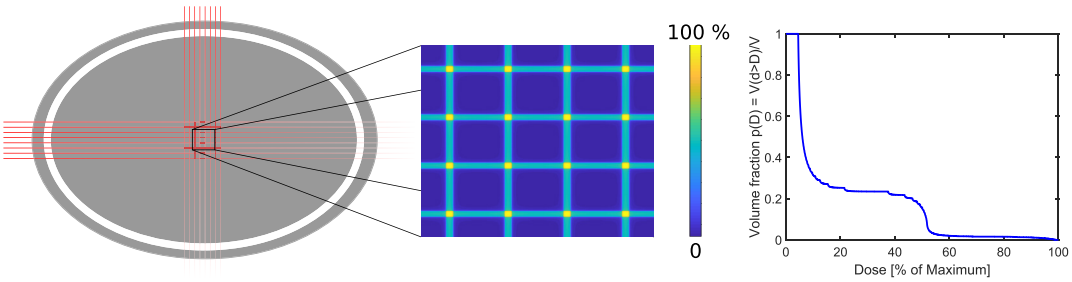

Figure 8. Voxel based dose volume histogram (right) for a cross firing geometry of microbeams (left).

beam direction, microbeam width and spacing and the visualisation of calculated treatment doses and parameters. The first MRT TPS was based on a PENELOPE Monte Carlo dose calculation engine (Martínez-Rovira *et al* 2012a). Debus *et al* (2017) presented the TPS VIRTUOS (Bendl *et al* 1994) with a kernel based dose calculation engine. Recently a hybrid dose calculation engine has been coupled to the popular TPS Eclipse (Varian) (Poole *et al* 2017) (see figure 9).

5. Multimodal MRT

While microbeam radiotherapy produces a unique way of selectively targeting cancerous tissues, further normal tissue sparing or tumour radio-sensitivity enhancement could be achieved with a multimodal approach combining MRT with nanoparticles (NPs) and/or chemotherapies.

The idea that the therapeutic index of MRT could be further improved by combining MRT irradiation with dose enhancers was first proposed by Dilmanian *et al* (2007). Synchrotron MRT beams in the 100 keV range are naturally prone to large absorption cross sections in elements with high atomic numbers, increasing secondary electron production associated mainly with the photoelectric effect. Contrast agents such as iodine, gadolinium or gold were proposed as possible candidates. Monte-Carlo simulated dose enhancement factors for MRT were obtained for different iodine, gadolinium and gold concentrations. A clear superiority was shown for gadolinium and gold with respect to iodine for dose enhancement in a human head phantom geometry (Prezado *et al* 2009). Other elements like thallium, lutetium or hafnium proved to also give satisfactory enhancements depending on the geometry of the irradiation (Martínez-Rovira and Prezado 2011).

If *in silico* analysis emphasized the interdependent roles of irradiation geometry, synchrotron beam energy and the choice of contrast agent material, the reality of *in vitro* and *in vivo* experiments add extra layers of constraints in the optimization problem. Tumour selectivity and specificity, injection modes and timing, contrast agents' size, micro- and macroscopic distribution, toxicity and retention, all become parameters of critical importance together with the choice of cell lines and animal models. Experimental verification of predicted dose enhancements is however crucial to demonstrate efficiency and better understand the underlying physical, chemical and biological mechanisms of interactions between the synchrotron microbeams and the dose enhancers.

Among other metallic high-Z NPs, gold NPs seem to be privileged candidates for multimodal MRT due to their relatively low intrinsic toxicity, high biocomptability and their capacity to diffuse and concentrate in tumours. Gokeri *et al* (2010) simulated that the hypothetical presence of 7 mg of gold per gram of tumour in a realistic head phantom irradiated with synchrotron microbeams would lead to substantial target dose increase allowing reduced skin, skull bone and maximum brain doses to produce the desired target dose. This dose increase was experimentally evidenced using normoxic polyacrylamide gels and bovine aortic endothelial cells exposed to 1mMol l^{-1} gold NPs (Rahman *et al* 2010). Interestingly, the gold NPs seem to influence the recovery rate of eradicated area *in vitro*, with a distinct behavior in favor of normal cells compared to cancerous ones which emphasizes once more a differential effect of MRT (Rahman *et al* 2011). In an *in vivo* experiment, Miladi *et al* (2014) showed that gold NPs coated by gadolinium chelates improved survival of synchrotron MRT treated rats bearing intracerebral 9L gliosarcoma (9LGS), an extremely radioresistant tumour.

Among the strong candidates, gadolinium based NPs are currently gaining popularity worldwide with the advances of image guided radiotherapy, in particular MRI guided radiation therapy delivery systems. Beyond their paramagnetic properties, the presence of the high-Z gadolinium atom makes them suitable as radiation dose enhancer. This was evidenced *in vivo* by Le Duc *et al* (2011) where rats bearing intracerebral 9LGS had their survival increased by a factor of five when gadolinium NPs were intravenously administered 20 minutes before their MRT treatment. Le Duc *et al* (2014) further demonstrated that more conventional gadolinium chelates did not appear to be of any benefit compared to AGuIX®, a gadolinium-based NP, that has now reached clinical trials with conventional radiation beams. Further optimization of the time sequence showed the radiosensitizing

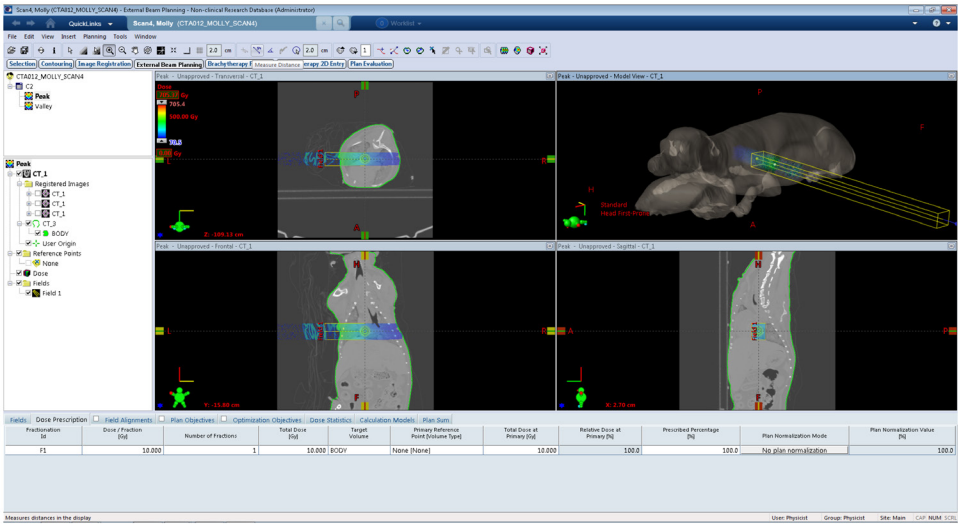

Figure 9. Treatment planning in preparation for pet clinical trials at the Australian Synchrotron with a combination Eclipse and the hybrid dose calculation.

effect of the gadolinium NPs is increased when MRT is delivered 24 h after injection, when the tumoral and cellular distributions of the NPs maximize lethal effects (Dufort *et al* 2016).

The importance of NPs' cellular distribution, especially in the unique spatially fractionated dose distributions of synchrotron microbeams, was also emphasized by Engels *et al* (2016) for the specific example of Tantalum pentoxide NPs. These non-toxic, nano-structured ceramic compounds were recently introduced as possible radiosensitizer and observed to form shells around cell nuclei instead of distributing homogeneously in the medium, producing remarkably different physical dose enhancements. This study showed that NP dose enhancement for synchrotron MRT is highly dependent on the NP congregation properties, location of congregations with respect to the beam peak, and photon energy.

In order to further improve the radiotherapeutic efficacy of MRT, other methods were developed by combining the effects of existing or novel anti-cancer drugs. If existing chemotherapy drugs like cisplatinum or temozolomide did not significantly improve the lifespan of the MRT treated rats with intracerebral 9L gliosarcoma, synergetic effects were observed *in vivo* using tubulin polymerization inhibitor JAI-51 (Bouchet *et al* 2012). The enhanced radio-sensitization of this antimetabolic drug was strongly correlated to G2/M phase cycle arrest. A major contributor to MRT efficacy is the immune response modulation (Bouchet *et al* 2013b). Smilowitz *et al* (2006) demonstrated that gene-mediated immunotherapy provides an important synergetic effect when combined with MRT, with almost 50% of the treated rats being long term survivors (>1 year). The preferential action of MRT on vascular network also lead to some other intrinsically linked radiation sensitization, immune function or chemotherapy efficacy improvement mechanisms, e.g. tumour oxygenation, which could be further exploited with anti-angiogenic agents (Griffin *et al* 2012).

In a more holistic approach, simultaneous use of chemotherapy drugs and NPs also opens the door to more complex theranostics aimed at image-guided and targeted selective lethal damages enhancement. Recent advances in the field of cancer therapy are focused on the design of novel drug delivery systems that feature therapeutic, diagnostic and imaging capabilities simultaneously. MRT will undoubtedly benefit from these advances.

6. Novel and future radiation sources

One of the main obstacles to the clinical translation of MRT is a lack of compact microbeam sources. Currently only a few large synchrotrons worldwide seem to be capable of generating the required beam properties. It is commonly accepted that the benefit of MRT over conventional RT critically depends on high PVDRs, low beam penumbras and sufficiently shallow dose fall-off with depth in order to treat deep seated tumours. Only radiation qualities that show little lateral scattering and generate short-ranged secondary particles are able to meet these criteria. Photon beams with kinetic energies between 100 keV and 300 keV seem to offer an acceptable compromise between low lateral scattering and low peak entrance doses when targeting deep seated tumours.

Apart from an appropriate radiation quality the source needs to provide low divergence and a source dimension which is smaller than the size of the generated beams, to ensure constant beam profiles with distance from the collimator and to keep beam penumbras small. Particularly challenging is the conservation of the micrometre sized dose profiles under the conditions of cardiovascular and respiratory motion in the traversed tissue.

Table 2. Inverse Compton scattering source projects with sources that provide more than 10^{12} ph s^{-1}. SR stands for storage ring, Linac for linear accelerator. The dose rate has been approximated assuming a field size of 20 mm^2 × 20 mm^2. Table adapted from Jacquet and Suortti (2015), reproduced with permission from Elsevier.

Project	Place	Type	E_X (keV)	Flux (ph s^{-1})	Source size (μm)	Dose rate (Gy s^{-1})
TTX	Beijing, China	SR	20–80	10^{12}	50	0.08
NESTOR	Kharkov, Ukraine	SR	30–500	10^{13}	70	6.6
ThomX	Orsay, France	SR	20–90	10^{13}	70	0.9
KEK QB	Tsukuba, Japan	Linac	35	10^{13}	10	1.5
KEK ERL	Tsukuba, Japan	Linac	67	10^{13}	30	0.8
MIT	Cambridge, USA	Linac	3–30	10^{14}	2	19

Radiation doses have to be applied within fractions of a second. Only a few large third generation synchrotrons are currently able to provide such high dose rates. However, radiobiological evidence for the requirement of dose rates in the 10 kGy range is still missing and *in vivo* experiments at lower dose rates have already successfully been carried out.

Third generation synchrotrons are large research facilities, with limited capacity for clinical studies in MRT and they are too expensive to be dedicated to cancer therapy alone. If MRT is to be established as a widespread radiotherapy treatment option, alternative compact microbeam sources need to be developed. Synchrotrons may demonstrate the principle feasibility of MRT, but are unlikely to provide widespread clinical applications.

6.1. Inverse Compton scattering sources

Promising and frequently discussed alternative radiation sources in MRT are inverse Compton scattering sources such as the Munich compact light source (Eggl *et al* 2016, Wright 2015). The principle of inverse Compton scattering is similar to synchrotrons. Instead of periodically deflecting electrons in static magnetic fields of undulators or wigglers, electrons interact with the electric field of a strong laser. Because the wavelength of emitted x-ray photons scales with the period of the wiggler field, lower electron energies are required to generate hard x-rays. The energy E_x of the emitted x-rays is approximately given by Loewen (2004)

$$E_x = 4\gamma^2 E_L \tag{3}$$

with a narrow spectrum.

Microbeams have been produced at the Munich Compact Light Source (MuCLS), the first commercially sold inverse Compton scattering source (Lyncean Technologies Inc., USA). The first *in vitro* studies were published (Burger *et al* 2017a) and currently *in vivo* studies in mice are being carried out (Burger *et al* 2017b, Dombrowsky *et al* 2019). MuCLS operates with a 4.6 m circumference storage ring with electrons of up to 45 MeV kinetic energy and produces photon energies between 15 and 35 keV. The source diameter is around 42 μm. First preclinical *in vitro* experiments used 25 keV photons with a dose rate of 1 Gy min^{-1} at 1.7 m distance from the source. Due to the low photon energies a 200 μm thick tungsten foil with 50 μm wide slits was sufficient to collimate microbeams with a pitch of 350 μm (Burger *et al* 2017a).

The future usability of inverse compton scattering sources for clinical applications in MRT depends on the possibility to upscale flux and photon energy of current machines. There are currently two designs investigated, linear accelerator based systems, which produce a slightly higher brilliance and storage ring based systems, such as MuCLS. Although linear accelerator based system offer a higher brilliance, storage ring based systems seem to be better suited for radiation therapy.

Despite substantial progress in the last years, Jacquet and Suortti (2015) estimate that even for ThomX, one of the most advanced systems being currently developed, the achieved dose rate will be in the order of a few Gy/min at an energy of up to 90 keV for clinically relevant field sizes. Table 2 shows currently developed inverse Compton scattering sources and their parameters.

6.2. Compact x-ray tube based microbeam sources

Conventional x-ray tubes are an abundantly available and inexpensive source of x-rays. In x-ray tubes electrons are accelerated to kinetic energies of up to several hundred keV and hit a target made of materials with high atomic numbers (usually tungsten). Interactions between electrons and target atoms generate bremsstrahlung and characteristic x-ray photons, which are emitted almost isotropically into a large solid angle. The efficiency of the conversion of electron beam energy into x-ray energy is very low in the order of around 1%. Most of the kinetic electron energy is converted into heat. To keep the surface temperature of the target below the melting point, the intensity of the electron beam in the focal spot is limited leading to a trade-off between focal spot (source) size and flux. Typical spot sizes are in the order of a few millimetre. As x-ray tubes deliver a strongly

divergent x-ray beam the dose rate is comparably low at reasonable distances from the focal spot. Hence, when using x-ray tubes for MRT, beam divergence close to the source, small relative output factors (ROF) and partial shadowing behind the collimator openings impair the microbeam field.

Several investigators developed compact microbeam systems for preclinical research (Babcock *et al* 2011, Bazyar *et al* 2017). However, most of these preclinical systems have larger aperture widths and should therefore rather be classified as minibeam systems. Fabrication of appropriate collimators is one of the most difficult steps in the development of x-ray tube based microbeam irradiators.

Recently, small animal radiotherapy platforms were developed to provide clinical standards in preclinical radiotherapy research, e.g. by establishing image guidance and treatment planning tools (Wong *et al* 2008). Such preclinical radiotherapy plattforms have recently also been used for the production of microbeams (or minibeams). Prezado *et al* (2017a) described a SARRP (Xstrahl Ltd, UK) based system with a 30 mm thick brass collimator that produced 400 to 500 μm wide beams with a centre to centre distance of around 1200 μm accounting for beam divergence. As the dose rate at the isocentre was too low they moved to 20 cm source distance and achieved 3.5Gy min^{-1} with a PVDR of around 12. With such a system they were able to achieve 58 Gy peak dose in a preclinical study with rats. In order to further increase the dose rate, they moved the sample off the isocentre closer to the source. Thus, unfortunately many of the features in the small animal radiotherapy platform are lost.

Esplen *et al* (2018) investigate possibilities to produce finer microbeams with 100 to 200 μm width at the SARRP isocentre and also tested a very simple collimator made of steel septa and double sided tape that produces 135 μm wide beams. They estimate the achievable peak dose to be roughly 90 Gy, assuming anesthesia to be limited to 1 h maximum.

A set-up that produces the typical microbeam configurations achieved at synchrotrons was presented by Bartzsch *et al* (2016). The authors used a tungsten collimator with divergent slits and achieved a dose rate of 10–18 Gy min^{-1} in only 6 cm distance from the focal spot of a 160 kVp x-ray tube. The PVDR of the 50 μm wide and 400 μm spaced beams was as high as 30, but depended strongly on the distance to the collimator. Due to the large divergence of the produced microbeams, the system was dedicated to *in vitro* research only.

6.3. Advanced x-ray tube technology

6.3.1. Carbon nanotube field emission technology

Schreiber and Chang (2012) investigated carbon nanotube field emission technology (CNT) as a mean to produce microbeams with x-ray tubes. In contrast to conventional thermionic electron emission requiring high cathode temperatures, CNT technology exploits high electric fields close to nanometer sized cathode structures to extract electrons at room temperature. The advantage of CNT cathodes over conventional thermionic cathodes are the achievable high electron current densities and small emittance (Shiffler *et al* 2004). Schreiber and Chang (2012) proposed a ring arrangement of anode segments around the patient as shown in figure 10. The electron beam is shaped to match the size of the projection of the collimator opening on the anode surface. A 10 cm thick single slit collimator with 100 μm slit width produced a single microbeam and by vertical translation between source and target several parallel microbeams can be applied. In Monte Carlo simulations they calculated the dose for a ring assembly of 24 cathode segments and estimated that such an assembly could deliver up to 280 Gy s^{-1}. Due to the ring geometry the entrance dose can be substantially reduced and reaches only 10% of the target dose. Moreover, they showed that a reduction of photon energy from 225 kVp to only 100 kVp has only minimal impact on the dose in the isocentre.

Hadsell *et al* (2013) presented a first prototype of a system with a 0.14 mm wide and 162 mm long focal track. With an acceleration voltage of 160 kV, 70 mA anode current they achieved a dose rate of 2 Gy s^{-1} in pulses of 0.1 s. A collimator produces a 300 μm wide beam. They apply these beams with 900 μm centre-to-centre spacing in a mouse experiment by shifting the sample holder and achieved 13 Gy peak entrance dose with a PVDR of 17. In another study they also demonstrate the feasibility of the ring shaped set-up (Hadsell *et al* 2014), although at much lower photon energy and dose rate.

However, until now there is no clinical system available and the microbeam width is rather in the minibeam domain. Whether such broader beams provide the same medical benefit as thinner beams needs to be validated. Moreover, the application of larger field in human sized targets may lead to substantially reduced PVDRs.

6.3.2. Line focus x-ray tube

Another recently developed concept is termed line focus x-ray tube (Bartzsch and Oelfke 2017). This concept suggests similarly a strongly eccentric focal spot on a rapidly rotating target. Monte Carlo simulations showed that such a system could provide a dose rate of 180 Gy s^{-1} in 0.5 m distance from the focal spot. At very high target surface velocities and high acceleration voltages, electron scattering is the dominant energy transport in the target instead of heat conduction. Consequently, heat capacity alone decides upon the focal spot temperature and a change in the focal spot width does not influence its temperature. Hence the focal spot width is only limited by lateral scattering of the electrons.

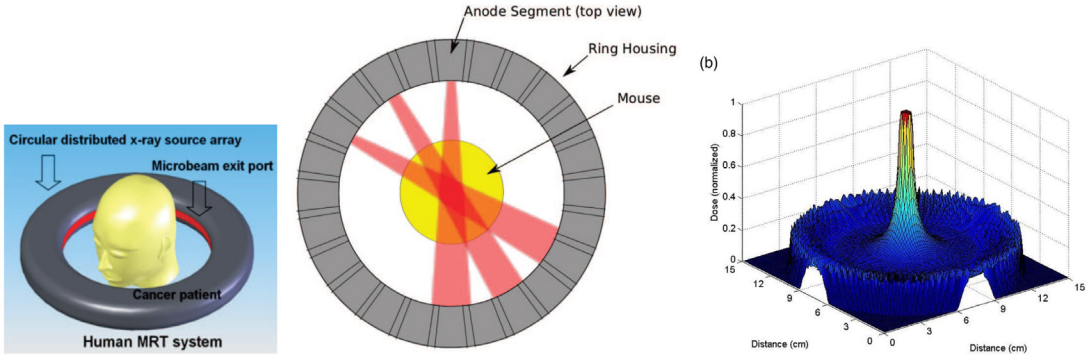

Figure 10. Ring geometry of carbon nanotube field emission technology x-ray tube developed by Schreiber and Chang (2012). The distribution of the source allows to create high peak doses in the isocentre while keeping the peak entrance dose low. Figure from Schreiber and Chang (2012) reproduced with permission of John Wiley & Sons.

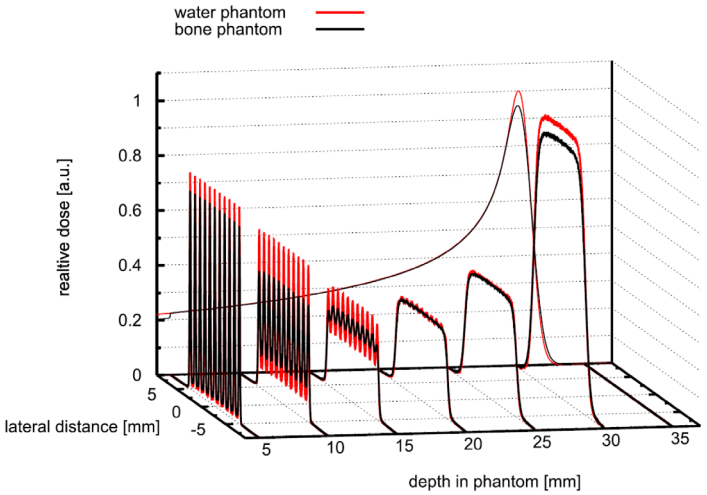

Figure 11. Simulated dose distribution of 60 MeV proton microbeams with 100 μm width and 1 mm spacing; figure from Kłodowska *et al* (2015) reproduced with permission of Elsevier. The phantom was either a homogeneous water cylinder (red) or a water cylinder with a bone slab (black). Dose distributions are normalised to their maximum. The background shows the mean depth dose curve.

Due to the small focal spot width the ROF becomes approximately 1. For a clinical system, Bartzsch *et al* (2016) suggested an acceleration voltage of 600 kV at a power of 1.5 MW. The maximum pulse length was estimated to be around 4 s delivering more than 700 Gy peak entrance dose. The higher mean photon energy of 150 keV will be advantageous for patient treatment due to a higher penentration depth. However, an experimental proof of concept remains outstanding.

6.4. Proton microbeams

Although research in MRT has primarily focused on photons, also particles have been investigated as a source for microbeams. Dilmanian and Meek (2010) proposed to use heavy ions for MRT but excluded protons from their patent, because they show strong lateral scattering. Nevertheless, particularly protons have recently gained attention, as proton beams are relatively easy to produce and shape. With depth these proton microbeams widen and the spatial dose modulation is lost in the Bragg peak region. In practice tissue sparing by dose modulation is achieved in the beam entrance region, whereas the tumour is treated with a conventional homogeneous dose as shown in figure 11. Hence, the technique is very similar to conventional proton therapy but with an additional normal tissue sparing effect in the beam entrance region.

Zlobinskaya *et al* (2013) were the first to introduce spatially fractionated radiation therapy with protons and proposed so called micro-channels: 10–50 μm wide pencil beams irradiated in a two dimensional grid with 500 μm spacing. Preclinical studies have shown that proton micro-channels lead to a similar tissue sparing effect as photon microbeams (Girst *et al* 2015).

Prezado and Fois (2013) investigated the possibility to use high energy protons of 1 GeV for the production of microbeams or minibeams. Since the range of 1 GeV protons is substantially larger than the size of a patient, the spatial modulation is preserved throughout the patient. However, currently only the Petersburg Nuclear Physics Institute, Russia, operates a synchrocyclotron capable of producing 1 GeV protons for medical applications. It is questionable whether laser accelerated particle sources will ever be compact and powerful enough to provide a reasonable alternative.

7. Conclusions

Access to suitable synchrotron light sources has limited MRT research to a small research community and has complicated the process of clinical translation until now. However, over time, a wealth of pre-clinical data has been acquired that impressively demonstrates the efficacy of microbeams in cancer treatment and also in neurological disorders such as epilepsy. The safe and responsible treatment of patients with microbeams requires solutions to several technological and medical physics challenges in MRT which are related to: the micrometre scale and gradient of the beams, the extremely high dose rates at synchrotrons, the low photon energy, and the development of compact alternative x-ray sources. This article reviewed these challenges and existing solutions. Despite these challenges, powerful dosimetry and dose calculation tools have been developed for MRT and are ready to use for first veterinary and human applications.

The need for treatment planning of micrometre sized radiation fields has led to the development of a range of dose calculation methods reviewed in chapter 4. Although Monte Carlo simulations are the standard for MRT dose calculation, the spatial dimensions required to score radiation doses render straight forward Monte Carlo solutions impractical for clinical applications. Appropriate scoring methods can reduce the number of required particle histories and curtail the amount of data. There exist also some alternative approaches to Monte Carlo techniques; particularly hybrid methods combining accurate Monte Carlo tools with fast convolution algorithms seem attractive.

A matter of debate is the clinically relevant radiation quantity that should be used for treatment planning, e.g. peak dose, valley dose or integrated dose. A promising approach may be the equivalent uniform dose (EUD) which relates inhomogeneous dose distributions to a homogeneous dose that would lead to equivalent cell survival. A final solution to this question requires further preclinical data and radiobiological models.

The high dose rate at synchrotrons poses a safety risk for patients, which needs to be handled reliably. Interlock systems and beam switches need to operate at high speed. At the European Synchrotron a patient safety system (PASS) was developed combining monitoring and shutter systems to handle these risks. To keep microbeam penumbras sharp, low photon energies of around 100 keV are used in MRT. The downside of such low photon energies are steep dose fall-offs with depth, known from early days of radiotherapy and treatments with orthovoltage radiation. A possible solution to this problem may be a concomitant treatment with dose enhancers such as gold or gadolinium nanoparticles, discussed in section 5. For treatment of patients the chosen photon energy spectrum needs to be a compromise between sharp beam penumbras and reasonable penetration depth.

Synchrotrons are likely to be the first place for clinical trials in MRT. Currently, the Australian and the European Synchrotron are investing in veterinary MRT trials as an intermediate step towards clinical applications in human patients. The purpose of veterinary trials—treating pet animals suffering from spontaneously growing tumours—is two-fold. Firstly, essential radiobiological data will be collected for both normal tissue toxicity and tumour control on a scale more closely resembling humans. Secondly, technological advancements, including treatment planning, image-guidance and patient positioning systems, will be tested, validated and refined for future clinical use.

In the long-term, clinical trials at large, synchrotron research facilities are logistically demanding. The widespread clinical use of MRT at synchrotrons is unlikely, although not impossible. Several promising alternative sources are under development and are already used for pre-clinical research. In the future, such sources could provide clinically suitable microbeams in a conventional hospital environment and convert MRT from an experimental method into a routinely deliverable treatment option. Furthest progressed are x-ray tube based concepts such as carbon nanotube cathode technology and line focus x-ray tubes, as they achieve dose rates of more than 100 Gy s^{-1} with appropriate photon energies.

To conclude, the promising therapeutic features of MRT are intrinsically tied to its distinct and demanding physical properties. The field of MRT has a clear clinical trajectory, however, the fulfilment of this pathway largely relies on advancements in medical physics. Although challenges undoubtedly remain, significant and encouraging progress has been made. With the continued development of suitable solutions for the challenging physics of x-ray microbeams, the first veterinary and human trials of MRT are within reach.

Acknowledgment

We dedicate this review article to the memory of Dr Elke Bräuer-Krisch (BE, PhD) who sadly passed away on 10 September 2018.

Elke was a central figure in Synchrotron MRT research and was known around the world for her outstanding contributions to the field, in particular MRT dosimetry.

ORCID iDs

Stefan Bartzsch https://orcid.org/0000-0001-9550-9122
Stéphanie Corde https://orcid.org/0000-0003-0388-7340
Mattia Donzelli https://orcid.org/0000-0002-1881-4331
Paolo Pellicioli https://orcid.org/0000-0003-3590-116X
Moeava Tehei https://orcid.org/0000-0003-3654-6833

References

ICRU Report 24 1976 *Determination of Absorbed Dose in a Patient Irradiated by Beams of X or Gamma Rays in Radiotherapy Procedures* (Washington, DC: International Commissionon Radiation Units and Measurements)

Akselrod G, Akselrod M, Benton E and Yasuda N 2006 A novel al2o3 fluorescent nuclear track detector for heavy charged particles and neutrons *Nucl. Instrum. Methods Phys. Res.* B **247** 295–306

Alaei P, Ding G and Guan H 2010 Inclusion of the dose from kilovoltage cone beam CT in the radiation therapy treatment plans *Med. Phys.* **37** 244–8

Alaei P, Gerbi B J and Geise R A 2000 Evaluation of a model-based treatment planning system for dose computations in the kilovoltage energy range *Med. Phys.* **27** 2821–6

Almaviva S *et al* 2010 Chemical vapor deposition diamond based multilayered radiation detector: physical analysis of detection properties *J. Appl. Phys.* **107** 014511

Andreo P, Burns D T, Hohlfeld K, Huq M S, Kanai T, Laitano F, Smythe V G and Vynckier S 2000 Absorbed dose determination in external beam radiotherapy *Technical Reports* Series No. 398, International Atomic Energy Agency, Vienna, Austria

Anton M 2005 Development of a secondary standard for the absorbed dose to water based on the alanine EPR dosimetry system *Appl. Radiat. Isot.* **62** 779–95

Anton M and Lelie S 2009 *Alanine Dosimetry: Uncertainty Components* (Berlin: Physikalisch-Technische Bundesanstalt Braunsweig)

Archer D W 1998 Collimator for producing an array of microbeams *US Patent* 5,771,270

Archer J, Li E, Davis J, Cameron M, Rosenfeld A and Lerch M 2019 High spatial resolution scintillator dosimetry of synchrotron microbeams *Sci. Rep.* **9** 6873

Archer J, Li E, Petasecca M, Dipuglia A, Cameron M, Stevenson A, Hall C, Hausermann D, Rosenfeld A and Lerch M 2017 X-ray microbeam measurements with a high resolution scintillator fibre-optic dosimeter *Sci. Rep.* **7** 12450

Archer J, Li E, Petasecca M, Stevenson A, Livingstone J, Dipuglia A, Davis J, Rosenfeld A and Lerch M 2018 Synchrotron x-ray microbeam dosimetry with a 20 μm resolution scintillator fibre-optic dosimeter *J. Synchrotron Radiat.* **25** 826–32

Babcock K, Sidhu N, Kundapur V and Ali K 2011 Collimator design for experimental minibeam radiation therapy *Med. Phys.* **38** 2192–7

Badal A and Badano A 2009 Accelerating Monte Carlo simulations of photon transport in a voxelized geometry using a massively parallel graphics processing unit *Med. Phys.* **36** 4878–80

Bartz J, Sykora G, Bräuer-Krisch E and Akselrod M 2011 Imaging and dosimetry of synchrotron microbeam with aluminum oxide fluorescent detectors *Radiat. Meas.* **46** 1936–9

Bartzsch S and Oelfke U 2013 A new concept of pencil beam dose calculation for 40–200 keV photons using analytical dose kernels *Med. Phys.* **40** 111714

Bartzsch S and Oelfke U 2017 Line focus x-ray tubes—a new concept to produce high brilliance x-rays *Phys. Med. Biol.* **62** 8600

Bartzsch S, Cummings C, Eismann S and Oelfke U 2016 A preclinical microbeam facility with a conventional x-ray tube *Med. Phys.* **43** 6301–8

Bartzsch S, Lerch M, Petasecca M, Bräuer-Krisch E and Oelfke U 2014 Influence of polarization and a source model for dose calculation in MRT *Med. Phys.* **41** 041703

Bartzsch S, Lott J, Welsch K, Bräuer-Krisch E and Oelfke U 2015 Micrometer-resolved film dosimetry using a microscope in microbeam radiation therapy *Med. Phys.* **42** 4069–79

Bayreder C, Georg D, Moser E and Berg A 2006 Basic investigations on the performance of a normoxic polymer gel with tetrakis-hydroxy-methyl-phosphonium chloride as an oxygen scavenger: reproducibility, accuracy, stability, and dose rate dependence *Med. Phys.* **33** 2506–18

Bazyar S, Inscoe C R, O'Brian E T, Zhou O and Lee Y Z 2017 Minibeam radiotherapy with small animal irradiators; *in vitro* and *in vivo* feasibility studies *Phys. Med. Biol.* **62** 8924

Belley M D, Stanton I N, Hadsell M, Ger R, Langloss B W, Lu J, Zhou O, Chang S X, Therien M J and Yoshizumi T T 2015 Fiber-optic detector for real time dosimetry of a micro-planar x-ray beam *Med. Phys.* **42** 1966–72

Bendl R, Pross J, Hoess A, Keller M, Preiser K and Schlegel W 1994 Virtuos-a program for virtual radiotherapy simulation and verification *Proc. of 11th Int. Conf. on The Use of Computers in Radiation Therapy (AR Hounsell ua Manchester: North Western Med. Physics Dept) pp* 226–7

Blattmann H *et al* 2005 Applications of synchrotron x-rays to radiotherapy *Nucl. Instrum. Methods Phys. Res.* A **548** 17–22

Bortfeld T, Schlegel W and Rhein B 1993 Decomposition of pencil beam kernels for fast dose calculations in three-dimensional treatment planning *Med. Phys.* **20** 311–8

Bouchet A, Boumendjel A, Khalil E, Serduc R, Bräuer E, Siegbahn E A, Laissue J A and Boutonnat J 2012 Chalcone jai-51 improves efficacy of synchrotron microbeam radiation therapy of brain tumors *J. Synchrotron Radiat.* **19** 478–82

Bouchet A, Bräuer-Krisch E, Prezado Y, El Atifi M, Rogalev L, Le Clec'h C, Laissue J A, Pelletier L and Le Duc G 2016 Better efficacy of synchrotron spatially microfractionated radiation therapy than uniform radiation therapy on glioma *Int. J. Radiat. Oncol. Biol. Phys.* **95** 1485–94
Bouchet A *et al* 2013a Synchrotron microbeam radiation therapy induces hypoxia in intracerebral gliosarcoma but not in the normal brain *Radiother. Oncol.* **108** 143–8
Bouchet A, Sakakini N, El Atifi M, Le Clec'h C, Brauer E, Moisan A, Deman P, Rihet P, Le Duc G and Pelletier L 2013b Early gene expression analysis in 9l orthotopic tumor-bearing rats identifies immune modulation in molecular response to synchrotron microbeam radiation therapy *PLoS One* **8** e81874
Bouchet A *et al* 2010 Preferential effect of synchrotron microbeam radiation therapy on intracerebral 9l gliosarcoma vascular networks *Int. J. Radiat. Oncol. Biol. Phys.* **78** 1503–12
Bouchet A *et al* 2017 Permeability of brain tumor vessels induced by uniform or spatially microfractionated synchrotron radiation therapies *Int. J. Radiat. Oncol. Biol. Phys.* **98** 1174–82
Bouchet A, Sakakini N, Atifi M E, Le Clec'h C, Bräuer-Krisch E, Rogalev L, Laissue J A, Rihet P, Le Duc G and Pelletier L 2015 Identification of areg and plk1 pathway modulation as a potential key of the response of intracranial 9l tumor to microbeam radiation therapy *Int. J. Cancer* **136** 2705–16
Bovée J V, Cleton-Jansen A M, Taminiau A H and Hogendoorn P C 2005 Emerging pathways in the development of chondrosarcoma of bone and implications for targeted treatment *Lancet Oncol.* **6** 599–607
Boyer A L and Cedric X Y 1999 Intensity-modulated radiation therapy with dynamic multileaf collimators *Seminars in Radiation Oncology* vol 9 (Amsterdam: Elsevier)
Brahme A 1984 Dosimetric precision requirements in radiation therapy *Acta Radiol.: Oncol.* **23** 379–91
Bräuer-Krisch E *et al* 2015 Medical physics aspects of the synchrotron radiation therapies: microbeam radiation therapy (MRT) and synchrotron stereotactic radiotherapy (ssrt) *Phys. Med.* **31** 568–83
Bräuer-Krisch E, Bravin A, Lerch M, Rosenfeld A, Stepanek J, Di Michiel M and Laissue J 2003 Mosfet dosimetry for microbeam radiation therapy at the european synchrotron radiation facility *Med. Phys.* **30** 583–9
Bräuer-Krisch E, Bravin A, Zhang L, Siegbahn E, Stepanek J, Blattmann H, Slatkin D, Gebbers J O, Jasmin M and Laissue J 2005a Characterization of a tungsten/gas multislit collimator for microbeam radiation therapy at the European synchrotron radiation facility *Rev. Sci. Instrum.* **76** 064303
Bräuer-Krisch E, Requardt H, Regnard P, Corde S, Siegbahn E, LeDuc G, Brochard T, Blattmann H, Laissue J and Bravin A 2005b New irradiation geometry for microbeam radiation therapy *Phys. Med. Biol.* **50** 3103
Bräuer-Krisch E, Nemoz C, Brochard T, Berruyer G, Renier M, Pouyatos B and Serduc R 2013 The preclinical set-up at the id17 biomedical beamline to achieve high local dose deposition using interlaced microbeams *J. Phys.: Conf. Ser.* **425** 022001
Bräuer-Krisch E, Requardt H, Brochard T, Berruyer G, Renier M, Laissue J and Bravin A 2009 New technology enables high precision multislit collimators for microbeam radiation therapy *Rev. Sci. Instrum.* **80** 074301
Bräuer-Krisch E, Serduc R, Siegbahn E A, Le Duc G, Prezado Y, Bravin A, Blattmann H and Laissue J A 2010 Effects of pulsed, spatially fractionated, microscopic synchrotron x-ray beams on normal and tumoral brain tissue *Mutation Res.* **704** 160–6
Brönnimann D, Bouchet A, Schneider C, Potez M, Serduc R, Bräuer-Krisch E, Graber W, Von Gunten S, Laissue J A and Djonov V 2016 Synchrotron microbeam irradiation induces neutrophil infiltration, thrombocyte attachment and selective vascular damage *in vivo Sci. Rep.* **6** 33601
Burger K *et al* 2017a Increased cell survival and cytogenetic integrity by spatial dose redistribution at a compact synchrotron x-ray source *PLoS One* **12** e0186005
Burger K *et al* 2017b Microbeam radiation therapy at a laser-based compact synchrotron x-ray source *Conf. on Lasers and Electro-Optics Europe European Quantum Electronics Conf. p* 1
Butler D J, Beveridge T, Lehmann J, Oliver C P, Stevenson A W and Livingstone J 2018 Spatial response of synthetic microdiamond and diode detectors measured with kilovoltage synchrotron radiation *Med. Phys.* **45** 943–52
Carlsson Å K and Ahnesjö A 2000 Point kernels and superposition methods for scatter dose calculations in brachytherapy *Phys. Med. Biol.* **45** 357
Cesari M, Bertoni F, Bacchini P, Mercuri M, Palmerini E and Ferrari S 2007 Mesenchymal chondrosarcoma. An analysis of patients treated at a single institution *Tumori J.* **93** 423–7
Cheung T, Butson M and Yu P 2009 Energy dependence corrections to mosfet dosimetric sensitivity *Australas. Phys. Eng. Sci. Med.* **32** 16–7
Cornelius I, Guatelli S, Fournier P, Crosbie J C, Sanchez del Rio M, Bräuer-Krisch E, Rosenfeld A and Lerch M 2014 Benchmarking and validation of a geant4-shadow Monte Carlo simulation for dose calculations in microbeam radiation therapy *J. Synchrotron Radiat.* **21** 518–28
Crosbie J C *et al* 2010 Tumor cell response to synchrotron microbeam radiation therapy differs markedly from cells in normal tissues *Int. J. Radiat. Oncol. Biol. Phys.* **77** 886–94
Crosbie J C, Fournier P, Bartzsch S, Donzelli M, Cornelius I, Stevenson A W, Requardt H and Braeuer-Krisch E 2015 Energy spectra considerations for synchrotron radiotherapy trials on the id17 bio-medical beamline at the European synchrotron radiation facility *J. Synchrotron Radiat.* **22** 1035–41
Crosbie J, Svalbe I, Midgley S, Yagi N, Rogers P W and Lewis R 2008 A method of dosimetry for synchrotron microbeam radiation therapy using radiochromic films of different sensitivity *Phys. Med. Biol.* **53** 6861
Davis J, Paino J, Dipuglia A, Cameron M, Siegele R, Pastuovic Z, Petasecca M, Perevertaylo V, Rosenfeld A and Lerch M 2018 Characterisation and evaluation of a pnp strip detector for synchrotron microbeam radiation therapy *BioMed. Phys. Eng. Express* **4** 044002
De Deene Y, Hurley C, Venning A, Vergote K, Mather M, Healy B and Baldock C 2002 A basic study of some normoxic polymer gel dosimeters *Phys. Med. Biol.* **47** 3441
De Felici M, Felici R, del Rio M S, Ferrero C, Bacarian T and Dilmanian F 2005 Dose distribution from x-ray microbeam arrays applied to radiation therapy: an egs4 Monte Carlo study *Med. Phys.* **32** 2455–63
De Felici M, Felici R, Ferrero C, Bravin A, Tartari A and Gambaccini M 2007 Monte carlo assessment of peak-to-valley dose ratio for MRT *Nucl. Instrum. Methods Phys. Res.* A **580** 489–92
De Felici M, Siegbahn E A, Spiga J, Hanson A L, Felici R, Ferrero C, Tartari A, Gambaccini M, Keyriläinen J and Bräuer-Krisch E 2008 Monte Carlo code comparison of dose delivery prediction for microbeam radiation therapy *J. Phys.: Conf. Ser.* **102** 012005
Debus C, Oelfke U and Bartzsch S 2017 A point kernel algorithm for microbeam radiation therapy *Phys. Med. Biol.* **62** 8341
Dilmanian F A and Meek A G 2010 Heavy ion therapy with microbeams *US Patent* App. 12/692,216
Dilmanian F A *et al* 2012 X-ray microbeam irradiation of the contusion-injured rat spinal cord temporarily improves hind-limb function *Radiat. Res.* **179** 76–88
Dilmanian F A, Morris G M and Hainfeld J F 2007 Methods for implementing microbeam radiation therapy *US Patent* 7,194,063

Dombrowsky A C et al 2019 Proof of principle experiment for microbeam radiation therapy at the Munich compact light source Radiat. Environ. Biophys. accepted
Donzelli M 2018 Improving dose calculation and treatment planning techniques for microbeam radiation therapy with computational methods PhD Thesis University of London
Donzelli M, Bräuer-Krisch E and Oelfke U 2016 Brain motion induced artefacts in microbeam radiation therapy: a Monte Carlo study Radiother. Oncol. 118 S34–5
Donzelli M, Bräuer-Krisch E, Nemoz C, Brochard T and Oelfke U 2016 Conformal image-guided microbeam radiation therapy at the esrf biomedical beamline id17 Med. Phys. 43 3157–67
Donzelli M, Bräuer-Krisch E, Oelfke U, Wilkens J J and Bartzsch S 2018 Hybrid dose calculation: a dose calculation algorithm for microbeam radiation therapy Phys. Med. Biol. 63 045013
Donzelli M, Oelfke U and Brauer-Krisch E 2019 Introducing the concept of spiral microbeam radiation therapy (spiralmrt) Phys. Med. Biol. 64 065005
Doran S J, Brochard T, Adamovics J, Krstajic N and Bräuer-Krisch E 2010 An investigation of the potential of optical computed tomography for imaging of synchrotron-generated x-rays at high spatial resolution Phys. Med. Biol. 55 1531
Dufort S et al 2016 The high radiosensitizing efficiency of a trace of gadolinium-based nanoparticles in tumors Sci. Rep. 6 29678
Duke P 2009 Synchrotron Radiation: Production and Properties vol 3 (Oxford: Oxford University Press)
Eggl E, Dierolf M, Achterhold K, Jud C, Günther B, Braig E, Gleich B and Pfeiffer F 2016 The Munich compact light source: initial performance measures J. Synchrotron Radiat. 23 1137–42
Elder F, Gurewitsch A, Langmuir R and Pollock H 1947 Radiation from electrons in a synchrotron Phys. Rev. 71 829
Emami B, Lyman J, Brown A, Cola L, Goitein M, Munzenrider J, Shank B, Solin L and Wesson M 1991 Tolerance of normal tissue to therapeutic irradiation Int. J. Radiat. Oncol. Biol. Phys. 21 109–22
Engels E, Corde S, McKinnon S, Incerti S, Konstantinov K, Rosenfeld A, Tehei M, Lerch M and Guatelli S 2016 Optimizing dose enhancement with ta 2 o 5 nanoparticles for synchrotron microbeam activated radiation therapy Phys. Med. 32 1852–61
Esplen N M, Chergui L, Johnstone C D and Bazalova-Carter M 2018 Monte Carlo optimization of a microbeam collimator design for use on the small animal radiation research platform (sarrp) Phys. Med. Biol. 63 175004
Fardone E et al 2018 Synchrotron-generated microbeams induce hippocampal transections in rats Sci. Rep. 8 184
Favaudon V et al 2014 Ultrahigh dose-rate flash irradiation increases the differential response between normal and tumor tissue in mice Sci. Trans. Med. 6 245ra93
Fournier P et al 2017 X-tream dosimetry of highly brilliant x-ray microbeams in the MRT hutch of the australian synchrotron Radiat. Meas. 106 405–11
Fournier P, Cornelius I, Donzelli M, Requardt H, Nemoz C, Petasecca M, Bräuer-Krisch E, Rosenfeld A and Lerch M 2016 X-tream quality assurance in synchrotron x-ray microbeam radiation therapy J. Synchrotron Radiat. 23 1180–90
Fraass B A 1995 The development of conformal radiation therapy Med. Phys. 22 1911–21
Gil S, Sarun S, Biete A, Prezado Y and Sabés M 2011 Survival analysis of f98 glioma rat cells following minibeam or broad-beam synchrotron radiation therapy Radiat. Oncol. 6 37
Girst S et al 2015 Improved normal tissue protection by proton and X-ray microchannels compared to homogeneous field irradiation Phys. Med. 31 615–20
Gokeri G, Kocar C and Tombakoglu M 2010 Monte Carlo simulation of microbeam radiation therapy with an interlaced irradiation geometry and an Au contrast agent in a realistic head phantom Phys. Med. Biol. 55 7469
Griffin R J, Koonce N A, Dings R P M, Siegel E, Moros E G, Bräuer-Krisch E and Corry P M 2012 Microbeam radiation therapy alters vascular architecture and tumor oxygenation and is enhanced by a galectin-1 targeted anti-angiogenic peptide Radiat. Res. 177 804–12
Hadsell M, Cao G, Zhang J, Burk L, Schreiber T, Schreiber E, Chang S, Lu J and Zhou O 2014 Pilot study for compact microbeam radiation therapy using a carbon nanotube field emission micro-CT scanner Med. Phys. 41 061710
Hadsell M et al 2013 A first generation compact microbeam radiation therapy system based on carbon nanotube x-ray technology Appl. Phys. Lett. 103 183505
Hall E J and Giaccia A J 2012 Radiobiology for the Radiologist (Philadelphia, PA: Lippincott Williams & Wilkins)
Hanson A, Slatkin D and Laissue J 2013 Unidirectional x-ray microbeam radiosurgery of infantile neuraxial malignancies: estimations of tolerable valley doses Photonic Therapeutics and Diagnostics IX vol 8565 (International Society for Optics and Photonics)
Hargrave D, Bartels U and Bouffet E 2006 Diffuse brainstem glioma in children: critical review of clinical trials Lancet Oncol. 7 241–8
Holsti L R 1995 Development of clinical radiotherapy since 1896 Acta Oncol. 34 995–1003
Hopewell J, Morris A and Dixon-Brown A 1987 The influence of field size on the late tolerance of the rat spinal cord to single doses of x rays Br. J. Radiol. 60 1099–108
Hugtenburg R P, Adegunloye A and Bradley D A 2010 X-ray microbeam radiation therapy calculations, including polarisation effects, with the Monte Carlo code egs5 Nucl. Instrum. Methods Phys. Res. A 619 221–4
Ibahim M J, Crosbie J C, Yang Y, Zaitseva M, Stevenson A W, Rogers P A and Paiva P 2014 An evaluation of dose equivalence between synchrotron microbeam radiation therapy and conventional broadbeam radiation using clonogenic and cell impedance assays PLoS One 9 e100547
Ibahim M, Yang Y, Crosbie J, Stevenson A, Cann L, Paiva P and Rogers P 2015 Eosinophil-associated gene pathways but not eosinophil numbers are differentially regulated between synchrotron microbeam radiation treatment and synchrotron broad-beam treatment by 48 h postirradiation Radiat. Res. 185 60–8
Irving D 1971 The adjoint Boltzmann equation and its simulation by Monte Carlo Nucl. Eng. Des. 15 273–93
Iván Lux L K 2000 Monte Carlo PARTICLE Transport Methods: Neutron and Photon Calculations (Boca Raton, FL: CRC Press)
Jacquet M and Suortti P 2015 Radiation therapy at compact compton sources Phys. Med. 31 596–600
Jia X, Gu X, Sempau J, Choi D, Majumdar A and Jiang S B 2010 Development of a gpu-based Monte Carlo dose calculation code for coupled electron–photon transport Phys. Med. Biol. 55 3077–86
Jia X, Yan H, Gu X and Jiang S B 2012 Fast Monte Carlo simulation for patient-specific CT/CBCT imaging dose calculation Phys. Med. Biol. 57 577–90
Kim K J 1986 Brightness, coherence and propagation characteristics of synchrotron radiation Nucl. Instrum. Methods Phys. Res. A 246 71–6
Kłodowska M, Olko P and Waligórski M 2015 Proton microbeam radiotherapy with scanned pencil-beams-Monte Carlo simulations Phys. Med. 31 621–6
Kron T, Duggan L, Smith T, Rosenfeld A, Butson M, Kaplan G, Howlett S and Hyodo K 1998 Dose response of various radiation detectors to synchrotron radiation Phys. Med. Biol. 43 3235–59
Kuznetsov S 2014 X-ray optics calculator www.ipmt-hpm.ac.ru/xcalc/xcalc/intro.php
Laissue J A et al 2013 Response of the rat spinal cord to x-ray microbeams Radiother. Oncol. 106 106–11

Laissue J A, Blattmann H and Slatkin D N 2012 Alban köhler (1874-1947): inventor of grid therapy *Z. Med. Phys.* **22** 90–9
Laissue J A *et al* 2001 Weanling piglet cerebellum: a surrogate for tolerance to MRT (microbeam radiation therapy) in pediatric neuro-oncology *Proc. SPIE* **4508** 65–73
Laissue J A *et al* 1998 Neuropathology of ablation of rat gliosarcomas and contiguous brain tissues using a microplanar beam of synchrotron-wiggler-generated x rays *Int. J. Cancer* **78** 654–60
Laissue J, Blattmann H, Wagner H, Grotzer M and Slatkin D 2007 Prospects for microbeam radiation therapy of brain tumours in children to reduce neurological sequelae *Dev. Med. Child Neurol.* **49** 577–81
Lazarakis P, Incerti S, Ivanchenko V, Kyriakou I, Emfietzoglou D, Corde S, Rosenfeld A B, Lerch M, Tehei M and Guatelli S 2018 Investigation of track structure and condensed history physics models for applications in radiation dosimetry on a micro and nano scale in geant4 *BioMed. Phys. Eng. Express* **4** 024001
Le Duc G *et al* 2011 Toward an image-guided microbeam radiation therapy using gadolinium-based nanoparticles *ACS Nano* **5** 9566–74
Le Duc G *et al* 2014 Advantages of gadolinium based ultrasmall nanoparticles versus molecular gadolinium chelates for radiotherapy guided by mri for glioma treatment *Cancer Nanotechnol.* **5** 4
Lerch M *et al* 2009 Multichannel silicon detectors for on-line synchrotron x-ray microbeam radiation dosimetry *10th Int. Conf. on Synchrotron Radiation Instrumentation (Melbourne)*
Lerch M, Petasecca M, Cullen A, Hamad A, Requardt H, Bräuer-Krisch E, Bravin A, Perevertaylo V and Rosenfeld A B 2011 Dosimetry of intensive synchrotron microbeams *Radiat. Meas.* **46** 1560–5
Lin Y, Liu T, Yang X, Wang Y and Khan M K 2013 Respiratory-induced prostate motion using wavelet decomposition of the real-time electromagnetic tracking signal *Int. J. Radiat. Oncol. Biol. Phys.* **87** 370–4
Livingstone J *et al* 2017 Preclinical radiotherapy at the australian synchrotron's imaging and medical beamline: instrumentation, dosimetry and a small-animal feasibility study *J. Synchrotron Radiat.* **24** 854–65
Livingstone J, Adam J F, Stevenson A, Hall C, Pelliccia D and Häusermann D 2015 Characterisation of a synthetic diamond detector for experimental dosimetry in MRT *Medical Applications of Synchrotron Radiation MASR*
Loewen R 2004 A compact light source: design and technical feasibility study of a laser-electron storage ring x-ray source *Technical Report* Stanford Linear Accelerator Center, Menlo Park, CA US (https://doi.org/10.2172/826755)
Low D A, Harms W B, Mutic S and Purdy J A 1998 A technique for the quantitative evaluation of dose distributions *Med. Phys.* **25** 656–61
Ma C M, Coffey C, DeWerd L, Liu C, Nath R, Seltzer S and Seuntjens J 2001 Aapm protocol for 40–300 kV x-ray beam dosimetry in radiotherapy and radiobiology *Med. Phys.* **28** 868–93
Mackie T, Scrimger J and Battista J 1985 A convolution method of calculating dose for 15 mV x rays *Med. Phys.* **12** 188–96
Manchado de Sola F, Vilches M, Prezado Y and Lallena A M 2018 Impact of cardiosynchronous brain pulsations on Monte Carlo calculated doses for synchrotron micro-and minibeam radiation therapy *Med. Phys.* **45** 3379–90
Marinelli M, Prestopino G, Verona C and Verona-Rinati G 2016 Experimental determination of the PTW 60019 microdiamond dosimeter active area and volume *Med. Phys.* **43** 5205–12
Marks L B, Yorke E D, Jackson A, Ten Haken R K, Constine L S, Eisbruch A, Bentzen S M, Nam J and Deasy J O 2010 Use of normal tissue complication probability models in the clinic *Int. J. Radiat. Oncol. Biol. Phys.* **76** S10–9
Martínez-Rovira I and Prezado Y 2011 Monte carlo dose enhancement studies in microbeam radiation therapy *Med. Phys.* **38** 4430–9
Martínez-Rovira I, Sempau J and Prezado Y 2012a Monte Carlo-based treatment planning system calculation engine for microbeam radiation therapy *Med. Phys.* **39** 2829–38
Martínez-Rovira I, Sempau J and Prezado Y 2012b Development and commissioning of a Monte Carlo photon beam model for the forthcoming clinical trials in microbeam radiation therapy *Med. Phys.* **39** 119–31
Maryanski M J, Gore J C, Kennan R P and Schulz R J 1993 Nmr relaxation enhancement in gels polymerized and cross-linked by ionizing radiation: a new approach to 3d dosimetry by mri *Magn. Reson. Imaging* **11** 253–8
Meyer J *et al* 2017 Biological and dosimetric characterisation of spatially fractionated proton minibeams *Phys. Med. Biol.* **62** 9260
Mijnheer B, Battermann J and Wambersie A 1987 What degree of accuracy is required and can be achieved in photon and neutron therapy? *Radiother. Oncol.* **8** 237–52
Miladi I *et al* 2014 The *in vivo* radiosensitizing effect of gold nanoparticles based mri contrast agents *Small* **10** 1116–24
Miura M, Blattmann H, Brauer-Krisch E, Bravin A, Hanson A, Nawrocky M, Micca P, Slatkin D and Laissue J 2006 Radiosurgical palliation of aggressive murine sccvii squamous cell carcinomas using synchrotron-generated x-ray microbeams *Br. J. Radiol.* **79** 71–5
Montay-Gruel P *et al* 2018 X-rays can trigger the flash effect: ultra-high dose-rate synchrotron light source prevents normal brain injury after whole brain irradiation in mice *Radiother. Oncol.* **129** 582–8
Montay-Gruel P *et al* 2017 Irradiation in a flash: unique sparing of memory in mice after whole brain irradiation with dose rates above 100 Gy s^{-1} *Radiother. Oncol.* **124** 365–9
Mukumoto N *et al* 2017 Sparing of tissue by using micro-slit-beam radiation therapy reduces neurotoxicity compared with broad-beam radiation therapy *J. Radiat. Res.* **58** 17–23
Nariyama N *et al* 2009 Spectromicroscopic film dosimetry for high-energy microbeam from synchrotron radiation *Appl. Radiat. Isot.* **67** 155–9
Nelson W R, Rogers D W O and Hirayama H 1985 The egs4 code system *Technical Report* SLAC report 265, Stanford University
Nemoz C, Kibleur A, Hyacinthe J N, Berruyer G, Brochard T, Brauer-Krisch E, Le Duc G, Brun E, Elleaume H and Serduc R 2016 *In vivo* pink-beam imaging and fast alignment procedure for rat brain tumor radiation therapy *J. Synchrotron Radiat.* **23** 339–43
Nettelbeck H, Takacs G J, Lerch M L F and Rosenfeld A B 2009 Microbeam radiation therapy: a Monte Carlo study of the influence of the source, multislit collimator, and beam divergence on microbeams *Med. Phys.* **36** 447–56
Niemierko A 1997 Reporting and analyzing dose distributions: a concept of equivalent uniform dose *Med. Phys.* **24** 103–10
O'connor J 1957 The variation of scattered x-rays with density in an irradiated body *Phys. Med. Biol.* **1** 352
Okada G, Morrell B, Koughia C, Edgar A, Varoy C, Belev G, Wysokinski T, Chapman D and Kasap S 2011 Spatially resolved measurement of high doses in microbeam radiation therapy using samarium doped fluorophosphate glasses *Appl. Phys. Lett.* **99** 121105
Okada G, Ueda J, Tanabe S, Belev G, Wysokinski T, Chapman D, Tonchev D and Kasap S 2014 Samarium-doped oxyfluoride glass-ceramic as a new fast erasable dosimetric detector material for microbeam radiation cancer therapy applications at the canadian synchrotron *J. Am. Ceram. Soc.* **97** 2147–53
Orion I, Rosenfeld A B, Dilmanian F A, Telang F, Ren B and Namito Y 2000 Monte Carlo simulation of dose distributions from a synchrotron-produced microplanar beam array using the EGS4 code system *Phys. Med. Biol.* **45** 2497–508
Pelliccia D, Crosbie J C and Larkin K G 2016a Phase contrast image guidance for synchrotron microbeam radiotherapy *Phys. Med. Biol.* **61** 5942

Pelliccia D, Poole C M, Livingstone J, Stevenson A W, Smyth L M, Rogers P A, Haüsermann D and Crosbie J C 2016b Image guidance protocol for synchrotron microbeam radiation therapy *J. Synchrotron Radiat.* **23** 566–73
Pellicioli P, Bartzsch S, Donzelli M, Krisch M and Bräuer-Krisch E 2019 High resolution radiochromic film dosimetry: comparison of a microdensitometer and an optical microscope *Phys. Med.* **65** 106–13
Petasecca M *et al* 2011 Dosimetry of intensive synchrotron microbeams *Radiat. Meas.* **46** 1560–5
Peucelle C, Nauraye C, Patriarca A, Hierso E, Fournier-Bidoz N, Martínez-Rovira I and Prezado Y 2015 Proton minibeam radiation therapy: experimental dosimetry evaluation *Med. Phys.* **42** 7108–13
Poole C M, Day L R, Rogers P A and Crosbie J C 2017 Synchrotron microbeam radiotherapy in a commercially available treatment planning system *BioMed. Phys. Eng. Express* **3** 025001
Poole C P 1996 Electron spin resonance: A comprehensive treatise of experimental techniques (New York: Dover Publications)
Pouyatos B *et al* 2013 Synchrotron x-ray interlaced microbeams suppress paroxysmal oscillations in neuronal networks initiating generalized epilepsy *Neurobiol. Dis.* **51** 152–60
Prezado Y and Fois G R 2013 Proton-minibeam radiation therapy: a proof of concept *Med. Phys.* **40** 031712
Prezado Y, Deman P, Varlet P, Jouvion G, Gil S, Le Clec' H C, Bernard H, Le Duc G and Sarun S 2015 Tolerance to dose escalation in minibeam radiation therapy applied to normal rat brain: long-term clinical, radiological and histopathological analysis *Radiat. Res.* **184** 314–21
Prezado Y *et al* 2017a Transfer of minibeam radiation therapy into a cost-effective equipment for radiobiological studies: a proof of concept *Sci. Rep.* **7** 17295
Prezado Y *et al* 2017b Proton minibeam radiation therapy spares normal rat brain: long-term clinical, radiological and histopathological analysis *Sci. Rep.* **7** 14403
Prezado Y, Fois G, Le Duc G and Bravin A 2009 Gadolinium dose enhancement studies in microbeam radiation therapy *Med. Phys.* **36** 3568–74
Prezado Y, Martínez-Rovira I and Sánchez M 2012a Scatter factors assessment in microbeam radiation therapy *Med. Phys.* **39** 1234–8
Prezado Y, Sarun S, Gil S, Deman P, Bouchet A and Le Duc G 2012b Increase of lifespan for glioma-bearing rats by using minibeam radiation therapy *J. Synchrotron Radiat.* **19** 60–5
Ptaszkiewicza M, Bräuer-Krisch E, Klosowski M, Czopyka L and Olkoa P 2008 Tld dosimetry for microbeam radiation therapy at the european synchrotron radiation facility *Radiat. Meas.* **43** 990–3
Raaymakers B *et al* 2017 First patients treated with a 1.5 t mri-linac: clinical proof of concept of a high-precision, high-field MRI guided radiotherapy treatment *Phys. Med. Biol.* **62** L41
Rahman W N, Davidson R, Yagi N, Bansal V, Geso M and Darby I 2011 Influence of gold nanoparticles on radiation dose enhancement and cellular migration in microbeam-irradiated cells *BioNanoScience* **1** 4–13
Rahman W N, Wong C J, Yagi N, Davidson R and Geso M 2010 Dosimetry and its enhancement using gold nanoparticles in synchrotron based microbeam and stereotactic radiosurgery *AIP Conf. Proc.* **1266** 107–10
Régnard P, Bräuer-Krisch E, Troprès I, Keyriläinen J, Bravin A and Le Duc G 2008 Enhancement of survival of 9l gliosarcoma bearing rats following intracerebral delivery of drugs in combination with microbeam radiation therapy *Eur. J. Radiol.* **68** S151–5
Renier M, Brochard T, Nemoz C and Thomlinson W 2002 A white-beam fast-shutter for microbeam radiation therapy at the ESRF *Nucl. Instrum. Methods Phys. Res.* A **479** 656–60
Renier M *et al* 2008 The radiotherapy clinical trials projects at the ESRF: technical aspects *Eur. J. Radiol.* **68** S147–50
Riedel R F, Larrier N, Dodd L, Kirsch D, Martinez S and Brigman B E 2009 The clinical management of chondrosarcoma *Curr. Treat. Opt. Oncol.* **10** 94–106
Romanelli P and Bravin A 2011 Synchrotron-generated microbeam radiosurgery: a novel experimental approach to modulate brain function *Neurological Res.* **33** 825–31
Romanelli P *et al* 2013 Synchrotron-generated microbeam sensorimotor cortex transections induce seizure control without disruption of neurological functions *PLoS One* **8** e53549
Rosenfeld A, Lerch M, Kron T, Bräuer-Krisch E, Bravin A, Holmes-Siedle A and Allen B 2001 Feasibility study of online high-spatial-resolution mosfet dosimetry in static and pulsed x-ray radiation fields *IEEE Trans. Nucl. Sci.* **48** 2061–8
Schreiber E C and Chang S X 2012 Monte Carlo simulation of a compact microbeam radiotherapy system based on carbon nanotube field emission technology *Med. Phys.* **39** 4669–78
Schültke E, Balosso J, Breslin T, Cavaletti G, Djonov V, Esteve F, Grotzer M, Hildebrandt G, Valdman A and Laissue J 2017 Microbeam radiation therapy—grid therapy and beyond: a clinical perspective *Br. J. Radiol.* **90** 20170073
Schültke E, Bräuer-Krisch E, Blattmann H, Requardt H, Laissue J and Hildebrandt G 2018 Survival of rats bearing advanced intracerebral f 98 tumors after glutathione depletion and microbeam radiation therapy: conclusions from a pilot project *Radiat. Oncol.* **13** 89
Schültke E *et al* 2008 Memory and survival after microbeam radiation therapy *Eur. J. Radiol.* **68** S142–6
Schültke E, Trippel M, Bräuer-Krisch E, Renier M, Bartzsch S, Requardt H, Döbrössy M D and Nikkhah G 2013 Pencilbeam irradiation technique for whole brain radiotherapy: technical and biological challenges in a small animal model *PLoS One* **8** e54960
Schulz-Ertner D, Jäkel O and Schlegel W 2006 Radiation therapy with charged particles *Seminars in Radiation Oncology* vol 16 (Amsterdam: Elsevier)
Schweiger A and Jeschke G 2001 *Principles of Pulse Electron Paramagnetic Resonance* (Oxford: Oxford University Press)
Serduc R, Berruyer G, Brochard T, Renier M and Nemoz C 2010a *In vivo* pink-beam imaging and fast alignment procedure for rat brain lesion microbeam radiation therapy *J. Synchrotron Radiat.* **17** 325–31
Serduc R *et al* 2010b High-precision radiosurgical dose delivery by interlaced microbeam arrays of high-flux low-energy synchrotron x-rays *PLoS One* **5** 1–12
Serduc R *et al* 2009 Synchrotron microbeam radiation therapy for rat brain tumor palliation—influence of the microbeam width at constant valley dose *Phys. Med. Biol.* **54** 6711
Serduc R *et al* 2008 Characterization and quantification of cerebral edema induced by synchrotron x-ray microbeam radiation therapy *Phys. Med. Biol.* **53** 1153
Serduc R *et al* 2006 *In vivo* two-photon microscopy study of short-term effects of microbeam irradiation on normal mouse brain microvasculature *Int. J. Radiat. Oncol. Biol. Phys.* **64** 1519–27
Shiffler D, Zhou O, Bower C, LaCour M and Golby K 2004 A high-current, large-area, carbon nanotube cathode *IEEE Trans. Plasma Sci.* **32** 2152–4
Siegbahn E A, Stepanek J, Bräuer-Krisch E and Bravin A 2006 Determination of dosimetrical quantities used in microbeam radiation therapy (MRT) with Monte Carlo simulations *Med. Phys.* **33** 3248–59
Siegbahn E, Bräuer-Krisch E, Bravin A, Nettelbeck H, Lerch M and Rosenfeld A B 2009 Mosfet dosimetry with high spatial resolution in intense synchrotron-generated x-ray microbeams *Med. Phys.* **36** 1128–37

Siegbahn E, Bräuer-Krisch E, Stepanek J, Blattmann H, Laissue J and Bravin A 2005 Dosimetric studies of microbeam radiation therapy (MRT) with Monte Carlo simulations *Nucl. Instrum. Methods Phys. Res.* A **548** 54–8
Siegel R L, Miller K D and Jemal A 2015 Cancer statistics *CA: Cancer J. Clinicians* **65** 5–29
Slatkin D N, Spanne P, Dilmanian F A, Gebbers J O and Laissue J A 1995 Subacute neuropathological effects of microplanar beams of x-rays from a synchrotron wiggler *Proc. Natl Acad. Sci. USA* **92** 8783–7
Slatkin D N, Spanne P, Dilmanian F and Sandborg M 1992 . Microbeam radiation therapy *Med. Phys.* **19** 1395–400
Smilowitz H *et al* 2006 Synergy of gene-mediated immunoprophylaxis and microbeam radiation therapy for advanced intracerebral rat 9l gliosarcomas *J. Neuro-Oncol.* **78** 135–43
Smyth L M, Donoghue J F, Ventura J A, Livingstone J, Bailey T, Day L R, Crosbie J C and Rogers P A 2018 Comparative toxicity of synchrotron and conventional radiation therapy based on total and partial body irradiation in a murine model *Sci. Rep.* **8** 12044
Soliman S Y S S, Pellicioli P, Beshira W, Abdel-Fattaha A A, Fahima R A, Krisch M and Bräuer-Krisch E 2019 A comparative dosimetry of alanine dosimeters with a PTW pinpoint chamber at ultra-high dose rates of synchrotron radiation *Phys. Med.* (submitted to)
Spiga J, Siegbahn E, Brauer-Krisch E, Randaccio P and Bravin A 2007a Geant4 simulations for microbeam radiation therapy (MRT) dosimetry *Nuclear Science Symp. Conf. Record* vol 4 (IEEE) pp 2571–75
Spiga J, Siegbahn E, Bräuer-Krisch E, Randaccio P and Bravin A 2007b The Geant4 toolkit for microdosimetry calculations: application to microbeam radiation therapy (MRT) *Med. Phys.* **34** 4322–30
Sprung C N, Yang Y, Forrester H B, Li J, Zaitseva M, Cann L, Restall T, Anderson R L, Crosbie J C and Rogers P A 2012 Genome-wide transcription responses to synchrotron microbeam radiotherapy *Radiat. Res.* **178** 249–59
Stepanek J, Blattmann H, Laissue J, Lyubimova N, Di Michiel M and Slatkin D 2000 Physics study of microbeam radiation therapy with psi-version of Monte Carlo code geant as a new computational tool *Med. Phys.* **27** 1664–75
Stevenson A W, Crosbie J C, Hall C J, Häusermann D, Livingstone J and Lye J E 2017 Quantitative characterization of the x-ray beam at the Australian synchrotron imaging and medical beamline (imbl) *J. Synchrotron Radiat.* **24** 110–41
Stupp R *et al* 2009 Effects of radiotherapy with concomitant and adjuvant temozolomide versus radiotherapy alone on survival in glioblastoma in a randomised phase iii study: 5 year analysis of the EORTC-NCIC trial *Lancet Oncol.* **10** 459–66
Sykora G J and Akselrod M S 2010 Novel fluorescent nuclear track detector technology for mixed neutron-gamma fields *Radiat. Meas.* **45** 594–8
Vahedi S *et al* 2012 X-ray induced Sm^{3+} to Sm^{2+} conversion in fluorophosphate and fluoroaluminate glasses for the monitoring of high-doses in microbeam radiation therapy *J. Appl. Phys.* **112** 073108
Van Der Sanden B, Bräuer-Krisch E, Siegbahn E A, Ricard C, Vial J C and Laissue J 2010 Tolerance of arteries to microplanar x-ray beams *Int. J. Radiat. Oncol. Biol. Phys.* **77** 1545–52
van Herk M 2007 Different styles of image-guided radiotherapy *Seminars in Radiation Oncology* vol 17 (Amsterdam: Elsevier)
Vozenin M C *et al* 2019 The advantage of flash radiotherapy confirmed in mini-pig and cat-cancer patients *Clin. Cancer Res.* **25** 35–42
Winick H and Doniach S 2012 *Synchrotron Radiation Research* (New York: Springer)
Wong J *et al* 2008 High-resolution, small animal radiation research platform with x-ray tomographic guidance capabilities *Int. J. Radiat. Oncol. Biol. Phys.* **71** 1591–9
Wright M D 2015 Microbeam radiosurgery: an industrial perspective *Phys. Med.* **31** 601–6
Wysokinski T W, Chapman D, Adams G, Renier M, Suortti P and Thomlinson W 2013 Beamlines of the biomedical imaging and therapy facility at the Canadian light source—part 2 *J. Phys.: Conf. Ser.* **425** 072013
Wysokinski T W, Chapman D, Adams G, Renier M, Suortti P and Thomlinson W 2015 Beamlines of the biomedical imaging and therapy facility at the canadian light source—part 3 *Nucl. Instrum. Methods Phys. Res.* A **775** 1–4
Yang Y, Crosbie J C, Paiva P, Ibahim M, Stevenson A and Rogers P A 2014 *In vitro* study of genes and molecular pathways differentially regulated by synchrotron microbeam radiotherapy *Radiat. Res.* **182** 626–39
Zagar T M *et al* 2017 Utility of deep inspiration breath hold for left-sided breast radiation therapy in preventing early cardiac perfusion defects: a prospective study *Int. J. Radiat. Oncol. Biol. Phys.* **97** 903–9
Zeman W, Curtis H and Baker C 1961 Histopathologic effect of high-energy-particle microbeams on the visual cortex of the mouse brain *Radiat. Res.* **15** 496–514
Zhang H *et al* 2008 Fractionated grid therapy in treating cervical cancers: Conventional fractionation or hypofractionation? *Int. J. Radiat. Oncol. Biol. Phys.* **70** 280–8
Zhang L, Yuan H, Burk L M, Inscoe C R, Hadsell M J, Chtcheprov P, Lee Y Z, Lu J, Chang S and Zhou O 2014 Image-guided microbeam irradiation to brain tumour bearing mice using a carbon nanotube x-ray source array *Phys. Med. Biol.* **59** 1283
Zlobinskaya O, Girst S, Greubel C, Hable V, Siebenwirth C, Walsh D W, Multhoff G, Wilkens J J, Schmid T E and Dollinger G 2013 Reduced side effects by proton microchannel radiotherapy: study in a human skin model *Radiat. Environ. Biophys.* **52** 123–33